HAL open science

# Near real-time management of spectral interferences with portable XRF spectrometers: Application to Sc quantification in nickeliferous laterite ores

Elodie Lacroix, Jean Cauzid, Yoram Teitler, Michel Cathelineau

▶ **To cite this version:**

Elodie Lacroix, Jean Cauzid, Yoram Teitler, Michel Cathelineau. Near real-time management of spectral interferences with portable XRF spectrometers: Application to Sc quantification in nickeliferous laterite ores. Geochemistry: Exploration, Environment, Analysis, 2021, pp.geochem2021-015. 10.1144/geochem2021-015 . hal-03315098

**HAL Id: hal-03315098**

**https://hal.univ-lorraine.fr/hal-03315098v1**

Submitted on 5 Aug 2021

**HAL** is a multi-disciplinary open access archive for the deposit and dissemination of scientific research documents, whether they are published or not. The documents may come from teaching and research institutions in France or abroad, or from public or private research centers.

L'archive ouverte pluridisciplinaire **HAL**, est destinée au dépôt et à la diffusion de documents scientifiques de niveau recherche, publiés ou non, émanant des établissements d'enseignement et de recherche français ou étrangers, des laboratoires publics ou privés.

Distributed under a Creative Commons Attribution 4.0 International License

Downloaded from http://geea.lyellcollection.org/ by GSL Maintenance User on July 26, 2021

Accepted Manuscript

*Geochemistry: Exploration, Environment, Analysis*

# Near real-time management of spectral interferences with portable XRF spectrometers: Application to Sc quantification in nickeliferous laterite ores

Elodie Lacroix, Jean Cauzid, Yoram Teitler & Michel Cathelineau

DOI: https://doi.org/10.1144/geochem2021-015

To access the most recent version of this article, please click the DOI URL in the line above. When citing this article please include the above DOI.

Received 22 February 2021
Revised 4 July 2021
Accepted 6 July 2021

© 2021 The Author(s). This is an Open Access article distributed under the terms of the Creative Commons Attribution 4.0 License (http://creativecommons.org/licenses/by/4.0/). Published by The Geological Society of London for GSL and AAG. Publishing disclaimer: www.geolsoc.org.uk/pub_ethics

Supplementary material at https://doi.org/10.6084/m9.figshare.c.5511838

**Manuscript version: Accepted Manuscript**
This is a PDF of an unedited manuscript that has been accepted for publication. The manuscript will undergo copyediting, typesetting and correction before it is published in its final form. Please note that during the production process errors may be discovered which could affect the content, and all legal disclaimers that apply to the journal pertain.

Although reasonable efforts have been made to obtain all necessary permissions from third parties to include their copyrighted content within this article, their full citation and copyright line may not be present in this Accepted Manuscript version. Before using any content from this article, please refer to the Version of Record once published for full citation and copyright details, as permissions may be required.

Downloaded from http://geea.lyellcollection.org/ by GSL Maintenance User on July 26, 2021

# Near real-time management of spectral interferences with portable XRF spectrometers: Application to Sc quantification in nickeliferous laterite ores

Elodie Lacroix[1], Jean Cauzid[1], Yoram Teitler[1] and Michel Cathelineau[1]

[1] Université de Lorraine, CNRS, CREGU, GeoRessources, 54506 Vandœuvre-lès-Nancy, France

*Corresponding author: elodie.lacroix@univ-lorraine.fr

## Abstract

Since the development of portable XRF (pXRF) spectrometers, few studies have been conducted on the influence of spectral interferences between chemical elements. This study aims to improve the management of these interferences to obtain more reliable geochemical analyses. We specifically investigate Ca-related interferences on Sc analysis for the case of Ni-rich laterite samples using the Niton XL3t GOLDD+ pXRF analyser. Three quantification methods were tested on 59 pelletised samples using the 'Soil' mode. The first named 'Manufacturer', represents the elemental quantification directly provided by the device based on Regions of Interest (ROI) and multilinear corrections of spectral interferences configured during the spectrometer design. The second, the '20 Cu' method, is based on spectral fitting using the PyMCA software. The third, the '18 Fe' method, combines spectral fitting with modified experimental conditions. For each, a quantification methodology was developed, establishing (i) Ca and Sc calibration lines and (ii) Ca/Sc threshold values delimiting fields of 'reliable', 'to be confirmed,' and 'unreliable' measurements. The '20 Cu' and '18 Fe' methods greatly extend the 'reliable measurements' field concerning the Ca/Sc ratio compared to the 'Manufacturer' method. The '18 Fe' method was also found to provide the most negligible measurement dispersion.

Keywords: portable XRF, spectral interference, scandium, calcium, nickel laterite, New Caledonia

"Supplementary materials are available at"

ACCEPTED MANUSCRIPT

Downloaded from http://geea.lyellcollection.org/ by GSL Maintenance User on July 26, 2021

**[Table A: Spectral characteristics (ROI ranges, Kα, Kβ spectral lines and escape peaks) for Ca, Sc, Ti, Mn and Fe analysis using pXRF, expressed in keV.**

*The ROI ranges are obtained by the NDT Alpha software relative to pXRF (NitonTM XL3t GOLDD+ of ThermoFisher ScientificTM) with the 'Soil' mode using the 'Low' filter (20 kV and Cu target). EDS resolution is 130 eV based on the Kα spectral line of Mn. For this study, the critical spectral interference is coloured blue-grey (Ca interfering with Sc), while other spectral interferences are coloured light grey (Sc with Ti and Fe with Mn).*

**Table B: Synthesis of the mineralogical and geochemical characteristics of the samples analysed in this study.**

**Figure A: XRF signal attenuation on the pellets with a thickness of 0.5 and 2 mm for the matrices of quartz ($SiO_2$) or hematite ($Fe_2O_3$).**

**Figure B: Determination of the optimal analytical conditions in the scandium spectral region for the pXRF analysis.**

*(a) Analysis of the optimal acquisition time of 30, 60, 90 and 120 seconds of the pXRF measurements on seven samples containing 71.7, 96.5, 117.5, 168.5, 185.9, 192.9 and 314.8 ppm of Sc determined with the whole-rock analysis by the SARM service.* Each boxplot is based on six pXRF measurements for each sample represented by circles and their whiskers.

***(b)*** *Analysis of the number of measurements necessary (from 3 to 8* randomly selected from a total of measurements*) to carry out on the same sample showing the evolution of measurement uncertainties (standard deviation) for the calibration analyses with pXRF. Example on a sample containing 117.5 ppm of Sc determined from whole-rock analysis by the SARM service.*

ACCEPTED MANUSCRIPT

Downloaded from http://geea.lyellcollection.org/ by GSL Maintenance User on July 26, 2021

**Figure C: Estimation of the tube current using several types of signal normalisation: Inelastic-scattering, Ar in K electron shell, Cu in K electron shell and Ag in L electron shell. These can be used as proxies for the current in the tube.**

**Figure D: Calibration lines for Ca with the '20 Cu' method (figure D.a) and with the '18 Fe' method (figure D.b).**

*Diamonds with black edges correspond to the 11 standards used to build the calibration line. Diamonds without an edge line correspond to the samples used for checking the calculated calibration line, and blue diamonds to standards or samples for which the average of their eight measurements falls within ±2$\sigma$ around the calibration curve. The red diamonds correspond to standards or samples for which the average of their eight measurements falls outside the ±2$\sigma$ interval around the calibration curve. The red diamonds in 2a correspond to samples with a >1% Ca content.*

**Figure E: The Ca/Sc threshold ratios defined for the '20 Cu' method (a) and the '18 Fe' method (b). For the '20 Cu' method (a), only one limit is visible (Limit 2 = 1822), which determines the field of the values where the Ca-Sc spectral interference is correctly resolved (below this limit) and the field of values where the spectral interference is never solved (above this limit). The same observation was made for the '18 Fe' method with a limit 2 = 2887 (b).**

*Diamonds with black edges correspond to the 11 standards used to build the calibration line. Diamonds without an edge line correspond to the samples used for checking the calculated calibration line. Blue diamonds correspond to standards or samples for which the average of their eight measurements falls within ±2$\sigma$ around the Sc-calibration curve. Red diamonds correspond to standards or samples for which the average of their eight measurements falls outside the ±2$\sigma$ interval around the Sc-calibration curve.*

**Figure F: Signal improvement for the quantification of Sc and Ca for an example of XRF spectrum (log scale of counts per second as a function of energy in keV) fitted with PyMCA (Solé et al., 2007)**

ACCEPTED MANUSCRIPT

Downloaded from http://geea.lyellcollection.org/ by GSL Maintenance User on July 26, 2021

**of the same laterite sample (containing 0.2% of Ca and 251.7 ppm of Sc) acquired with three pXRF spectrometers. The energy range is from 3 to 7 keV in the scandium spectral region for the pXRF analysis.**

*(a) Spectrum acquired using the '20 Cu' method (purple curve) and the '18 Fe' method (green curve) for the same analysis time (90 seconds) in an energy range from 3 to 7 keV; (b) Zoom on this spectrum in an energy range from 3 to 5 keV showing the spectral lines of Ca and Sc (Ca-Ka, Ca-Kb and Sc-Ka).*]

ACCEPTED MANUSCRIPT

Downloaded from http://geea.lyellcollection.org/ by GSL Maintenance User on July 26, 2021

## Introduction

X-ray-fluorescence (XRF) is a non-destructive and multi-element analytical technique routinely used to characterise the chemistry of rocks, minerals, sediments, fluids and soils (Lemiere et al., 2014; Young et al., 2016; Andrew and Barker, 2018; Tian et al., 2018; Kim et al., 2019). Several types of XRF spectrometers have been developed, including miniaturised portable X-ray fluorescence (pXRF) analysers. However, the first pXRFs with multi-element capabilities have been commercially available since 1979 (Glanzman and Closs, 2007). Furthermore, since the innovation of the SDD (Silicon Drift Detector) detector in 1991 (Forster *et al*., 2011 in Cao et al., 2016; Lemière, 2018), pXRF analysers have benefited from rapid technical developments and found various applications for environmental (Laperche, 2005; Lemiere et al., 2014; Ribeiro et al., 2017; Arantes de Carvalho et al., 2018) and archaeological purposes (Sanoit (de) et al., 2005; Conrey et al., 2014; Frahm, 2017) and in the field of mineral resource sciences (Konstantinov and Strujkov, 1995; Le Vaillant et al., 2014; Hall et al., 2016; Gisbert et al., 2021). pXRF analysers provide cheap, relatively fast geochemical measurements to explore mineral resources and are now routinely used in the field. In this context, several studies have been conducted to assess pXRF analysers' capabilities to analyse various mineral ores. The objective was to improving and guide the use of pXRFs in mineral resource exploration (Gazley et al., 2011; Gazley et al., 2011; Fisher et al., 2014; Hall et al., 2014; Cao et al., 2016; Sarala, 2016; Gazley et al., 2017; Andrew and Barker, 2018; Hughes and Barker, 2018).

In XRF spectroscopy, several sources of errors have to be managed to efficiently quantify the elemental content of samples (Beckhoff et al., 2006). Some artefacts are related to the detector characteristics and include spectral interferences (Thompson, et al., 2001; Sanoit (de) et al., 2005; Conrey et al., 2014; Hall et al., 2014; Quiniou & Laperche, 2014; Ibáñez-Insa et al., 2017), pileup and escape peaks (Van Espen et al., 1980; Thompson, et al., 2001; Conrey et al., 2014). Others artefacts such as secondary and higher-order fluorescence are linked to the sample's matrix. The secondary X-ray fluorescence stimulation of a chemical element is caused by the fluorescence of another element

ACCEPTED MANUSCRIPT

Downloaded from http://geea.lyellcollection.org/ by GSL Maintenance User on July 26, 2021

present in the sample, such as Fe fluorescence exciting Cr, or Ni fluorescence exciting Fe (Thompson, et al., 2001; Beckhoff et al., 2006). Among these phenomena, spectral interference produced by an abundant element on a trace element remains challenging to manage using a pXRF (Conrey et al., 2014; Hall et al., 2014; Le Vaillant et al., 2014; Piercey and Devine, 2014; Gazley et al., 2017; Ibáñez-Insa et al., 2017). Most solid-state detector response function in spectrometers such as the pXRF requires a decomposition of the spectrum which is achieved by approximating fluorescence peaks by mathematical functions. The fluorescence signal itself has a Lorentz distribution but it is convolved by the detector response, which has a Gaussian distribution. The resulting function has a Voigt distribution although the Gaussian part dominates the signal, indicating that an initial approach of decomposing spectra using Gaussian functions may be sufficient. A Voigt function, approximated with a pseudo-Voigt would be preferable for more detailed works (Van Espen et al., 1980; Solé et al., 2007). These mathematical functions are added to a baseline which can be evaluated with polynomial iterative moving averages (Statham, 1976) and Sensitive Nonlinear Iterative Peak (Ryan et al., 1988). Mathematical functions add up on the baseline and are adjusted using a least-square fitting (Whiting, 1968; Van Espen et al., 1980). On laboratory devices, the elemental quantification of samples is performed after data acquisition by using this kind of spectral decomposition supervised by expert staff. However, portable devices process data during acquisition in real-time without any input from the user which means that spectral decomposition is not feasible and pXRF spectrometers usually calculate element concentrations based on regions of interest (ROI). ROIs correspond to specific spectral bandwidths in which the detected signal is mainly linked to a single specific element. The spectral overlapping of X-ray emission, secondary fluorescence and for some devices escape peaks is tabulated in a matrix acting as a multilinear correction for the intensities detected in each ROI. Sum peaks are automatically limited in pXRF by a current regulation in the tube controlled by the count rate in the detector. They are, therefore, of limited influence on the calculation of elemental concentration. The quantification of trace elements in the presence of spectrally interfering major elements remains problematic. Such interferences limit the capabilities

ACCEPTED MANUSCRIPT

Downloaded from http://geea.lyellcollection.org/ by GSL Maintenance User on July 26, 2021

of pXRF analysers, particularly in mineral exploration (e.g., Hall et al., 2014). Few studies have specifically investigated the influence of spectral interferences on calculations of element concentrations (Gallhofer and Lottermoser, 2018).

This study aims to develop and optimise the quantification of trace elements in the presence of more concentrated spectrally interfering elements. It was applied to nickel-bearing laterites from New Caledonia and conducted with a Niton Xl3t GOLDD+. Figure 1 shows a spectral comparison of the same sample analysed by two pXRFs - the Niton, which automatically corrects escape peaks (Figure 1a) and the XMET, which does not correct escape peaks before spectral processing (Figure 1b and 1c). The automatic correction of the escape peak of the Fe-Kα emission line with the Niton (red vertical line in Figure 1) leads to the deformation of the baseline, which is only visible on log scale spectra. For a major element such as Ti-Kα, this effect is minor but is greater than the Sc-Kβ signal. With the XMET, the escape peak can be evaluated afterwards on a smoother baseline. Still, the escape peak thus represents another spectral interference that needs to be solved (Figures 1b and 1c). Hence, in both cases, the escape peak affects the quantification of a trace element (Sc) which is already impacted by the signal of a major element (Ti). A similar effect is observed for the Mn-Kα escape peak on the Sc-Kα and Ca-Kβ emission lines. Investigations here were devoted to evaluating the influence of the spectral interference caused by Ca on Sc estimates due to the proximity between the Kα spectral line of Sc and the Kβ spectral line of Ca (Thompson, et al., 2001; Hall et al., 2014; Figure 1; Table A in Supplementary material). The multilinear regression corrections mathematically reflect the phenomenon of secondary fluorescence on the ROIs of the interfering elements. However, the effect of this phenomenon decreases from V to Ca and it becomes negligible for the Sc quantification compared to its spectral interference with Ca (Thompson et al., 2001). Other essential parameters have been considered, such as the analysis mode and the data processing method (Quiniou & Laperche, 2014; Ross et al., 2014).

This contribution presents an easy-to-apply solution that enables discrimination between measurements that have been correctly cleaned of spectral interferences and those requiring

ACCEPTED MANUSCRIPT

Downloaded from http://geea.lyellcollection.org/ by GSL Maintenance User on July 26, 2021

further correction. Three processing methods that require increasing data processing skills are proposed. The first method (named 'Manufacturer') consisted of reading the data directly on the spectrometer, in which elemental quantification is based on ROIs. The built-in pXRF programme solves spectral interferences by applying multilinear corrections. The second method (named '20 Cu') is based on the spectral fitting of the data using the PyMCA software. Spectral interferences are solved by decomposing spectra using mathematical functions added to a baseline evaluation. These first two methods were carried out using the manufacturer's experimental conditions. The final method (named '18 Fe') was based on spectral fitting using PyMCA from spectra acquired with modified experimental conditions - the voltage in the X-ray tube and the secondary X-ray source.

## Geological setting

New Caledonia hosts world-class Ni-rich laterites, which developed after intense weathering of peridotites following Late Eocene obduction (Cluzel et al., 2001; Ulrich et al., 2020). Recently, economically attractive Sc (≈ 100 ppm) concentrations have been noted in New Caledonian Ni laterites (Audet, 2008; Teitler et al., 2019; Ulrich et al., 2019) which means that Sc may become a valuable by-product of Ni- and Co-ore processing. Some laterised amphibolite dykes, locally intruding into the peridotite, have elevated Sc concentrations up to 300 ppm and may constitute standalone Sc targets (Teitler et al., 2019). Above the peridotite bedrock in New Caledonia, Ni-rich laterite profiles typically consist of a succession of weathering facies including (from bottom to top) rocky saprolite, earthy saprolite, yellow laterite, red laterite and ferruginous duricrust. Unweathered peridotite and rocky saprolite are dominated by magnesium-rich silicates, whereas iron oxides-oxyhydroxides mainly dominate earthy saprolite, yellow/red laterite and duricrust horizons. Laterised amphibolites differ from laterised peridotites in that they contain significant amounts of kaolinite and gibbsite together with iron oxides-oxyhydroxides (Teitler et al., 2019).

## Materials and methods

ACCEPTED MANUSCRIPT

Downloaded from http://geea.lyellcollection.org/ by GSL Maintenance User on July 26, 2021

***Whole-rock geochemical analysis***

Forty-three samples collected at five mining sites and encompassing three types of lithologies (weathered peridotites, weathered amphibolites, unweathered amphibolites) were selected for pXRF analysis. Hand specimens were crushed using an agate bowl pulveriser at the GeoRessources Laboratory. Pulps were analysed at the SARM analytical service using standard procedures (CRPG Laboratory, following Carignan et al., 2001). Major element oxides and Sc were determined using an iCap6500 ICP-OES with Li borate fusion. Trace elements were determined using an iCapQ ICP-MS through the nitric acid digestion of fused beads. Loss on ignition (LOI) was determined on separate aliquots by drying sample powders overnight at 110°C, ignition at 980°C and subsequent measurement of the weight loss. The analytical accuracy (2 standard deviations) lies within the typical uncertainty of the analytical data for both major and trace elements, namely less than 1% for major elements and less than 5% for most trace elements. Detailed procedures and limits of detection and quantification are given on the facility website (https://sarm.cnrs.fr/index.html). Scandium and Ca concentrations in the investigated samples vary from 44 to 315 ppm and from 0.01 to 9.4 wt.%, respectively. Selected samples correspond to three lithologies: (i) strongly weathered peridotites (Group 1), (ii) fresh to weakly weathered amphibolites (Group 2) (iii) strongly weathered amphibolites (Group 3). Group 1 was made up of earthy saprolite, yellow and red laterite derived from peridotites and was the most enriched in $Fe_2O_3$ (44.7-73.0 wt.%), the most $SiO_2$ depleted (0.8-21.0 wt.%), with $Al_2O_3$ ranging from 3.0 to 10.3 wt.%. The CaO content of weathered peridotites was low (< 0.01-0.40 wt.%), and the Sc content was low to moderate (44-97 ppm). Group 2 yielded the lowest $Fe_2O_3$ content (7.4-27.9 wt.%) together with the highest $SiO_2$ content (30.8- 48.1 wt.%). The $Al_2O_3$ content varied between 4.4 and 14.9 wt.%, CaO was high (4.9-13.0 wt.%), and Sc content ranged from 75 to 212 ppm (Teitler et al., 2019). Compared to Group 1, Group 3 was less enriched in $Fe_2O_3$ (24.5-55.9 wt.%), had higher $SiO_2$ and $Al_2O_3$ (5.7-35.9 wt.% and 6.0-23.9 wt.% respectively), moderate CaO content (< 0.01-2.8 wt.%) and a high Sc content (118-315 ppm) (Teitler et al., 2019). The whole-rock geochemical dataset is given in Table B in the supplementary material.

ACCEPTED MANUSCRIPT

Downloaded from http://geea.lyellcollection.org/ by GSL Maintenance User on July 26, 2021

### *Sample preparation for pXRF analysis*

The selected field samples are representative of the lateritic profile. This kind of profile is marked by abrupt compositional changes that lead to samples clustered as groups in the Ca vs Sc space. However, this study focuses on establishing a methodological approach to quantify a trace element, here Sc,whose the emission line of is overlapped by that of a major element, Ca. As the detection limit for Sc in those samples was not known at the start of the study, we decided to create composite samples of intermediate composition by mixing field samples to get a more distribution of the measurements in the Ca vs Scdiagrams. Thus, 16 additional samples were prepared by mixing weighted quantities of the collected samples. In total, fifty-nine samples were used for this study (Figure 2).

Powdered samples were formed into 12.4 mm-wide pellets using a 10-tons hydraulic press. A powder mass of between 0.6 and 0.8 g was used to ensure a minimum thickness of 2 mm and to prevent pellet degradation over time. Pellets were analysed without using any film between the sample and the spectrometer. This experimental procedure optimises the signal obtained on light and trace elements (Hall et al., 2014; Adams et al., 2020). Analytical calculations performed with the dedicated module in PyMCA indicate that X-ray absorption through iron oxide samples thicker than 0.5 mm is at least $10^{-6}$ on the 1-8 keV energy range, which is the energy range of interest in this study (Figure A in Supplementary materials). Therefore, using 2 mm-thick samples ensures that samples suit the infinite-thickness model as assumed by the pXRF algorithm.

### *pXRF*

The pXRF used in this study is the Niton™ XL3t GOLDD+, manufactured by ThermoFisher Scientific™. Its X-ray tube consists of a silver anode operating under a maximum voltage of up to 50 kV. The Silicon Drift Detector (SDD) has an active area of 25 $mm^2$ and provides a spectral resolution of 130

ACCEPTED MANUSCRIPT

Downloaded from http://geea.lyellcollection.org/ by GSL Maintenance User on July 26, 2021

eV at the Mn-Kα emission line (based on the Full Width at Half Maximum (FWHM) at 5.899 keV). Pelletised samples were analysed using a beam of 8 mm in diameter.

A pXRF analysis is a two-step process. First, spectra are acquired with controlled analytical conditions and subsequently processed to convert the signals into elemental concentrations. A single measurement displayed on the screen of a pXRF usually corresponds to several analytical conditions. These conditions consist of a specific voltage in the tube and a foil between the tube and the sample. The purpose of the foil is to selectively cut some of the tube signal and/or act as a secondary source. Analytical conditions are named 'beams' in some devices and 'filters' for the Niton series. Four filters are available in the Xl3t for geological applications: Main, Low, High and Light. Each filter is dedicated to measuring a specific set of elements. Quantification of Sc is carried out using the Low filter. Unsurprisingly, tests done on the Main, Low and Light filters to assess the quality of the Sc signal in the corresponding analytical conditions have proved that the Low filter was the one that provides the best signal to noise ratio. The Low filter consists of a voltage of 20 kV in the tube, generating a beam passing through a Cu-coated foil before reaching the sample. The absorption edge of the K-shell of Cu is 8.98 keV. The Cu foil acts as a secondary source with Cu K-emission lines effectively absorbed by the K-shell electrons for the elements ranging from K to Co. Fe contents can be very high in lateritic samples and lead to a strong escape peak of Fe interfering with Ti. The Xl3t automatically corrects escape peaks, but that correction is not perfect and may lead to 'downward peaks' that modify the baseline on which fluorescence peaks are built (Figure 1a).

A new filter was developed to remove that effect which involved using the Fe foil available in the Xl3t. The X-ray fluorescence of Fe from the foil cannot generate fluorescence of Fe in the sample which means the Fe signal, including its escape peak, is therefore drastically reduced. As a positive side-effect, removing the Fe signal decreased the count rate in the detector, thus leading to an automatic increase of the current in the tube, which led to higher Ca and Sc signals (Figure F in Supplementary materials). Moreover, the X-ray fluorescence of Fe was more intensely absorbed by Ca and Sc compared to the Cu X-ray fluorescence, which thus further improved the signal to noise

ACCEPTED MANUSCRIPT

Downloaded from http://geea.lyellcollection.org/ by GSL Maintenance User on July 26, 2021

ratio on these elements. The absorption edge of the K-shell of Fe is 7.11 keV, which is ~2 keV below that of Cu (8.98 keV). The efficiency of the emission of the secondary source depends on the difference in energy between the signal emitted by the tube and the absorption edge of the element of which the foil is made. Therefore, the voltage in the tube was decreased by 2 kV so that conditions remained comparable to those of the Low filter. The new filter, thus consisted of an 18 kV voltage in the tube and a Fe-coated foil acting as secondary source. The precise composition and thickness of foils in the Xl3t are usually not provided to users by Thermo Scientific, unlike other manufacturers.

The second step of pXRF measurements is the conversion of signal intensities to elemental concentrations. In this process, the device first evaluates the signal emitted by each element to be quantified. All portable devices use the same approach to evaluate spectra and display results on the screen during the measurement. The signal from an energy range corresponding to an element is integrated. Energy ranges are called Regions of Interest (ROI). For one element, its ROI value is linearly corrected from the contribution of the signal of all the other elements in the same ROI, which means the spectral interferences can be taken into account. An alternative solution is to evaluate a baseline and decompose the signal above the baseline using mathematical functions such as Gaussians or pseudo-Voigt least-square fitted to the experimental signal. In this way, the signal from an element corresponds to the function area and is free of interferences. However, users are usually not provided with this solution, even off-line. In this study, the ROI and decomposition solutions were investigated.

Once the signal of one element is evaluated, the conversion into concentrations can be carried out using two classes of algorithms in portable devices. The first is Compton Normalization, which corresponds to the 'Soil' mode in the Xl3t (Brand & Brand, 2014). Compton Normalization is based on a specific matrix type, here Si-rich and Al-rich soils (Mussini, 2009; Margui and Van Grieken, 2013; Brand & Brand, 2014; Conrey et al., 2014; Quiniou & Laperche, 2014; Lemière, 2018). In the 'Soil' mode, only samples similar to the matrix used to normalise the signal can be quantified. The Xl3t

ACCEPTED MANUSCRIPT

Downloaded from http://geea.lyellcollection.org/ by GSL Maintenance User on July 26, 2021

uses three filters (Main, Low, High) and quantifies Sc. However, applying Compton Normalization to lateritic samples dominated by Fe oxides may lead to biased results. The second mode corresponds to a Fundamental Parameter approach (Brand & Brand, 2014), which uses a complete physical model to correct matrix effects and quantify elemental concentrations in most geological samples. These modes include four filters - Main, Low, High, Light. However, the Mining mode in the Xl3t available for this study does not include Sc.

In this paper, results read from the spectrometer using the 'Low' filter in the 'Soil' mode are referred to as 'Manufacturer'. These results, determined by the built-in pXRF programme, are based on evaluating the signal using ROIs. In parallel, spectra obtained with the Low filter and processed as areas of pseudo-Voigt using PyMCA are referred to as '20 Cu'. Finally, results extracted from spectra obtained with the Fe-coated foil excited by an 18 kV voltage in the tube and processed to evaluate the signal as areas of pseudo-Voigt are referred to as '18 Fe' (Table 1).

***The optimal conditions for pXRF analysis***

To determine the optimal analytical conditions in the scandium spectral region, several metrological tests were conducted before establishing calibration lines such as reproducibility and duration measurements. The reproducibility of XRF analysis was assessed through repeated measures and monitoring of any slow or sudden drift of the spectrometer measurements (Brand & Brand, 2014; Gazley and Fisher, 2014; Gazley et al., 2017). The optimal acquisition time is the best compromise between accuracy and precision on the one hand, and the acquisition time on the other (Fisher et al., 2014; Hall et al., 2014; Piercey and Devine, 2014; Ross et al., 2014). Several durations (30 s, 60 s, 90 s and 120 s) were used with the 'Low' filter in 'Soil' mode for two weathered peridotite samples and five weathered amphibolite samples, to assess the precision of the Sc analysis. These samples cover the whole range of the analysed Sc concentrations from the overall sample set, with 72, 97, 118, 169, 186 and 315 ppm. The 120 s and 90 s acquisition times led to pXRF values close to those

ACCEPTED MANUSCRIPT

Downloaded from http://geea.lyellcollection.org/ by GSL Maintenance User on July 26, 2021

obtained from whole-rock ICP-AES analysis. Hence, a duration of 90 s per acquisition was chosen for the following (Figure B.a in Supplementary materials).

Furthermore, an additional test was conducted to assess the measurement accuracy. This evaluation identifies the optimal number of analyses that need to be carried out on the same sample to minimise error and increase the associated accuracy. The associated uncertainty was calculated as twice the standard deviation. Monitoring of the standard deviation with an increasing number of repeated analyses (from 3 to 12) indicates that the decrease in the standard deviation value becomes marginal when repeatedly measuring the same sample more than eight times (Figure B.b in Supplementary materials). Consequently, each sample was measured eight times with a 90 s acquisition time. The pellet was laid on the spectrometer nose for each analysis, using the manufacturer's analytical stand.

***Software***

Raw data (spectra) and interpreted data (element contents) were transferred from the pXRF analyser using the NDT software developed by ThermoFisher. In addition, the NDT Alpha software from ThermoFisher was used to build a specific User Method loaded into the pXRF which provided the '18 Fe' method excitation conditions.

Spectral decomposition in the '20 Cu' and '18 Fe' methods was carried out using the PyMCA software developed by the European Synchrotron Radiation Facility (ESRF, Solé et al., 2007). This software manages peak fitting by considering emission line ratios and includes sum peaks and escape peaks (Figure 1). Hence, the interferences detailed above were solved and the signal for each element was estimated as the area of the function chosen for the least-square fitting. The function used with the PyMCA software is the pseudo-Voigt, an approximation of the Voigt, characterised by the sum of a Gaussian with a Lorentzian function with the same position and area (Whiting, 1968). The pseudo-Voigt was preferred to the Gaussian as the former provided a better fit of the base of a

ACCEPTED MANUSCRIPT

Downloaded from http://geea.lyellcollection.org/ by GSL Maintenance User on July 26, 2021

single peak. Such a choice was necessary because the weak Sc signals add to the high-energy base of the strong Ca signal (Figure 1c).

### *Quantification methods*

The XRF technique offers several approaches that can be used to obtain quantitative results, which can be divided into two main classes: compensation methods (dilution, internal standard, standard addition, Compton scatter) and matrix correction methods (fundamental parameters, empirical influence coefficient, theoretical influence coefficient) (Lachance and Claisse, 1995; Sitko and Zawisza, 2012; Piercey and Devine, 2014). All these methods require some knowledge of chemical analysis or XRF spectroscopy. In this study, we intend to construct a method that can be implemented by users who are not experts in XRF and therefore we used calibration curves. These curves have been determined from standards which are samples of a known chemical composition similar to that of the sample to be assayed (Laperche, 2005; Arne et al., 2014; Gazley and Fisher, 2014; Le Vaillant et al., 2014; Sarala, 2016; Gazley et al., 2017; Andrew and Barker, 2018; Hughes and Barker, 2018; Lemière, 2018). In our study, 11 samples were used as standards. They were chosen to i) group together a range in which most of the samples were contained in the Ca-Sc space (Figure 2), ii) include some reference samples inside this group, iii) limit the number of standards to a small amount.

The pXRF devices automatically adapt the current in the tube to reach an optimal dead time, meaning that elemental signals obtained from spectra must be normalised to the tube current to become comparable. The device automatically performs such an operation for its internal quantification, and therefore, no manual normalisation is required for the 'Manufacturer' method. However, normalisation still needs to be carried out for the '20 Cu' and '18 Fe' methods and the NDT software does not provide this information. Although the NDT_Alpha software provides this information, we decided to evaluate this from the spectrum. Scattered data from the specific emission lines of Ag from the anode of the tube and scattering of the bremsstrahlung of the tube or

ACCEPTED MANUSCRIPT

Downloaded from http://geea.lyellcollection.org/ by GSL Maintenance User on July 26, 2021

the Ar signal were among the possible solutions available. Under the selected analytical conditions, Ag does not emit fluorescence on its K-lines because the voltage in the tube is too low. The Ag L-lines are absorbed by the Cu- or Fe-foils and cannot be scattered by the sample. Scattering of the bremsstrahlung can be measured at ~16 keV where there is no signal emitted from the sample, but this requires an extra processing step. The Ar signal arises from the air layer between the tube and sample. As pellets of similar geometry are analysed, the thickness of that air layer is constant and the Ar signal is directly proportional to the current in the tube. The plot of these signals against the current in the tube is provided as supplementary material in Figure C. As Ar, Ca and Sc can be measured simultaneously, Ar-peak normalisation was chosen in this study (Menez, 1999; Cauzid, 2005; Shao et al., 2020).

The calibration curve must be established using reference samples that are accurately measured with the pXRF. This recommendation is not guaranteed as some reference samples have a low Sc content or high Ca/Sc ratios. Hence, a series of reference samples were selected for which the pXRF data could be expected to be accurate. The chosen criteria were: i) an Sc concentration of at least 100 ppm, well above the detection limit for Sc as advocated by the manufacturer (Sc LoD is 75 ppm within the Si-Ca-Fe matrix according to Niton data), ii) a limited Ca-Kβ/Sc-Kα interference with a Ca-Kβ emission line intensity of around ten times the emission of the Sc-Kα line. To roughly evaluate the second condition, the Ca Kβ emission line was considered to be ~10 times less intense than its Kα emission line. The Ca concentration of these samples was limited to 1% given this ratio and because the minimum Sc concentration of the reference samples used during this first step was 100 ppm. A first calibration curve was drawn from the four samples which satisfied these Sc (>100 ppm) and Ca (<1%) conditions. This first calibration curve was defined with a zero intercept. Next, the standard deviation was calculated from the 32 measurements available for these four samples. Standards whose average value fell within plus or minus twice this standard deviation were selected in a second step to calculate the calibration line with a non-zero intercept. Following these steps allowed

ACCEPTED MANUSCRIPT

Downloaded from http://geea.lyellcollection.org/ by GSL Maintenance User on July 26, 2021

us to automatically exclude the reference samples that were not accurately measured by the pXRF due to spectral interferences between the Ca-Kβ and Sc-Kα emission lines.

## Results

Figure 3 shows the calibration curves defined by linear regression of the data obtained with the 'Manufacturer' method. The Sc concentrations directly provided by the pXRF are not equal to the actual Sc concentrations obtained by the SARM service analysis. The first evaluation of the calibration curve with a zero intercept has a determination coefficient of 0.67. In contrast, the final calibration line has a slope of 2.45, an intercept of -89.96 and a determination coefficient of 0.84. The limit of determination, i.e. the lowest concentration that can be determined, was defined as the concentration for which the errors become equal or greater than the concentration. The error was evaluated as being twice the standard deviation. Using this evaluation, the limit of determination for Sc with the Manufacturer method is 79 ppm.

Moreover, some standards and sample values do not have an average value within a ±2σ interval around the regression line (Figure 3a). For Ca, the final calibration line has a slope of 0.93, an intercept of 1058.44 and a determination coefficient of 0.998 (Figure 3b). Therefore, the limit of determination for Ca with the Manufacturer method is 2500 ppm. The dispersion of the results for each standard or sample increases according to the Ca concentration. Hence, the 2σ value calculated on the whole dataset overestimates dispersion at lower values, so Ca is most probably correctly quantified at concentrations below 2500 ppm.

Only one of the standards was not correctly quantified for Sc. It is included in the graph on the upper limit of the confidence interval (y=ax+b+2σ line). Therefore, the Sc content of this sample (80 ppm) is at the limit of determination for Sc. All of the other incorrectly quantified standards and samples stand on or below the lower limit of the confidence interval (y=ax+b-2σ line).

ACCEPTED MANUSCRIPT

Downloaded from http://geea.lyellcollection.org/ by GSL Maintenance User on July 26, 2021

Figure 4 was drawn up to investigate the importance of the Ca-Kβ spectral interference on estimation of Sc pXRF concentrations. It shows the deviation from the calibration line in ppm, calculated as the difference between the whole-rock Sc concentrations, and pXRF Sc values ($Sc_{whole\ rock}$ - $Sc_{manufacturer}$) as a function of the intensity of the spectral interference, calculated as the ratio between the Ca and Sc concentrations ($Ca_{Manufacturer}/Sc_{manufacturer}$). The average $Sc_{whole\ rock}$ - $Sc_{manufacturer}$ value for each set of eight reliable measurements on a standard or sample should be between +2σ and -2σ. Samples standing below the lower limit of the confidence interval (y=ax+b-2σ line) have values lower than -79 ppm on the ordinate axis in Figure 4. Conversely, samples standing above the upper limit of the confidence interval (y=ax+b+2σ line) have values higher than 79 ppm on the ordinate axis. All samples standing on or below the lower limit of the confidence interval in Figure 3 have high ($Ca_{Manufacturer}/Sc_{manufacturer}$) in Figure 4. They also have Ca concentrations above 1 wt.% (Figure 5).

Figure 4 shows three fields defined by two limits. Limit 1 is set at the lowest Ca/Sc ratio value obtained on an incorrectly quantified standard. Limit 2 is set at the highest Ca/Sc ratio value obtained on an accurately measured standard. In the green field below Limit 1 (Ca/Sc values below 67), Sc concentrations of standards are systematically correctly evaluated (Limit 1). Scandium concentrations of standards may or may not be correctly assessed in the orange field between Limit 1 and Limit 2 (Ca/Sc values ranging from 67 to 104). Finally, in the red field above Limit 2 (Ca/Sc values above 104), Sc concentration is systematically over-evaluated (Figure 4).

Two samples are located in a non-adapted coloured field (Figure 4). The sample with 80 ppm Sc at upper values of the confidence interval under the LoD in Figure 3 corresponds to the series of red points following the upper limit (y=ax+b-2σ) dotted-point-line at 80 ($Sc_{whole\ rock}$ – $Sc_{Manufacturer}$) on Figure 4, with Ca/Sc values ranging from 0 to 1800. Another sample is located below Limit 1 while not being correctly quantified (Figure 4). It corresponds to the sample at lower values of the confidence interval in Figure 3 with a Sc concentration of 265 ppm.

ACCEPTED MANUSCRIPT

Downloaded from http://geea.lyellcollection.org/ by GSL Maintenance User on July 26, 2021

The Limit 1 and Limit 2 threshold ratios, together with the Sc-LoD, can be represented in a Ca vs Sc biplot, thus defining three fields (Figure 5). The green field (reliable measurements), situated below Limit 1 and above the Sc-LoD, corresponds to Sc values that are always correctly evaluated. The orange field above the Sc-LoD, and between Limit 1 and Limit 2, corresponds to Sc values that may or may not be correctly assessed. The red field (erroneous measurements), above Limit 2 or below the Sc-LoD, corresponds to Sc values that are never accurately evaluated. Calcium and Sc concentrations obtained from whole-rock and pXRF analysis are also presented in Figure 5 to show the accuracy and precision of pXRF estimates compared to whole-rock data. For each of the analysed standards and samples, Ca and Sc concentrations are represented by a cross-linked to a black dot. The black dot corresponds to the whole-rock values. The cross shows the minimum and maximum values obtained for Ca and Sc using pXRF. Calcium and Sc concentrations obtained with the 'Manufacturer' method have been converted to actual concentrations using calibration lines as defined in Figure 3. In the green field, Sc pXRF estimates are consistent with concentrations obtained from the whole-rock analysis, whereas Sc is systematically overestimated in the red field (Figure 5). The sample plotted horizontally in Figure 4 at the upper limit ($y=ax+b-2\sigma$) could not be shown in Figure 5 as the Sc concentrations calculated using the regression line led to negative Sc values.

The Sc calibration lines for the '20 Cu' and '18 Fe' methods are given in Figure 6. The precision of the Sc values is significantly better using the '18 Fe' method ($2\sigma$ = 51 ppm) than the '20 Cu' method ($2\sigma$ = 84 ppm). Fitting the data with pseudo-Voigt functions enabled us to estimate accurate Sc values when using the '20 Cu' method (Figure 6a). With the '18 Fe' method (Figure 6b), only one sample does not exhibit correct estimation of the Sc content due to a Ca content above 3 wt.%.

The calibration lines for Ca and (($Sc_{whole\ rock}$ – Sc) vs (Ca/Sc)) diagrams for the '20 Cu' and '18 Fe' methods are available in Figures D and E of the 'Supplementary material' section. These two methods correctly evaluated all standards. Therefore, only one limit was determined, namely Limit 2 at Ca/Sc = 1822 for the '20 Cu' method and at Ca/Sc = 2887 for the '18 Fe' method. Hence, the field

ACCEPTED MANUSCRIPT

Downloaded from http://geea.lyellcollection.org/ by GSL Maintenance User on July 26, 2021

between Limit 1 and Limit 2, which included a mixture of accurate and inaccurate results, could not be drawn. Therefore, two fields are evident: 'Reliable values' in green and 'Unreliable values' in red.

In the Ca vs Sc biplots for the '20 Cu' method, all the processed analyses are above the Sc-LoD and fall within the ± 2σ interval (± 84 ppm) from the calibration line, i.e., within the reliable measurements' field (in green on Figure 7a). On the other hand, the '18 Fe' method (Figure 7b) shows only one sample (3.5 wt.% Ca and 212 ppm Sc) on the entire dataset that is outside of the ± 2σ interval.

## Discussion

In the following, we shall first discuss the causes for the discrepancy between Sc concentrations directly provided by the pXRF ('Manufacturer' method) and actual Sc concentrations obtained from the whole-rock analysis. We shall then discuss the relevance of the different methods regarding the analytical precision and management of the spectral interference caused by Ca.

### *Slope of the Sc calibration line*

The slope of the Sc-calibration line obtained with the 'Manufacturer' method (i.e., Sc concentrations directly provided by the pXRF; Figure 3) is about twice the expected 1:1 slope. Such an anomalously elevated calibration slope may be related to the use of the 'Soil' mode. The 'Soil' mode quantification process is based on a Compton Normalization and calibrated for a silico-aluminous matrix (Hall et al., 2014; Quiniou & Laperche, 2014; Ross et al., 2014). In the present case, the analysed samples are dominated mainly by iron oxides. Establishing this type of correlation using the 'Mining' mode based on Fundamental Parameter algorithms would have probably resulted in a slope closer to one (Hall et al., 2014; Quiniou & Laperche, 2014). However, the current manufacturer configuration for the Niton™ XL3t GOLDD+ available for this study only allows Sc quantification through the 'Soil' mode. A standard user cannot access the internal parameters and algorithms of

ACCEPTED MANUSCRIPT

Downloaded from http://geea.lyellcollection.org/ by GSL Maintenance User on July 26, 2021

the different pXRF analytic modes (Brand & Brand, 2014) and, as such, cannot add an element into a specific mode.

***Optimisation of analytical precision***

The repetitive analysis of selected standards provides helpful information regarding measurement precision. The 2σ error is calculated for Sc with the whole set of standards and not as the average of the 2σ interval for each standard. Values obtained with the 'Manufacturer' and the '20 Cu' methods are similar (79 and 84 ppm, respectively). In contrast, the '18 Fe' method was found to improve the precision with the 2σ interval decreasing to 50 ppm. A better understanding of the source of errors in the spectral fitting process is required to improve analytical precision. Spectral decomposition in pseudo-Voigt functions is built upon a baseline evaluated from the spectrum (Figure 1). Firstly, the baseline calculation is sensitive to the noise visible as high-frequency variations in the spectrum (Solé et al., 2007; Tian et al., 2009; Margui and Van Grieken, 2013). Secondly, escape peaks are automatically corrected with the Niton XL3t device. This correction cannot always be optimal and sometimes generates sharp spectral artefacts peaking down on the spectrum. These peaks are of limited depth and become visible using a logarithmic vertical scale. However, they slightly influence the baseline position and the least square fitting of the pseudo-Voigt. Thirdly, low-frequency background noise, mainly from Compton and Bremsstrahlung's physical phenomena, also affects the baseline. The nature of some secondary sources (Al, Ti, Zr, Mo and W) can influence the latter phenomenon (Tian et al., 2009).

The noise appears as sharp peaks up and sharp peaks down. These can be seen at low energy on Figures 1a and 1b and the position of the automatically corrected Fe-escape peak in Figure 1a. Although these do not appear as sharp peaks on more intense emission lines (Ca, Ti, Fe-escape on Figure 1c), they still slightly modify the peak shape. The exact position of sharp peaks up and sharp peaks down, or the modification of peak shapes changes from one measurement to the next. The least-square fitting calculates the difference between the experimental value and the value of the

ACCEPTED MANUSCRIPT

Downloaded from http://geea.lyellcollection.org/ by GSL Maintenance User on July 26, 2021

pseudo-Voigt in each channel, squares the difference and finally sums the squares. The process then modifies the pseudo-Voigt height to minimise the sum of squares of the differences. The height of the pseudo-Voigt will then depend on the exact shape of the noise, which changes with each measurement. This noise influence will be more significant for peaks of lower intensity, such as that of Sc. Hence the noise has a substantial impact on peak areas used to build the calibration curve in the '20 Cu' and '18 Fe' methods. On the contrary, ROIs integrate the signal over a significant width, which will end in an almost constant value from one measurement to the next, making ROIs less sensitive to noise. The consequence of this is the higher dispersion observed with the '20 Cu' method ($2\sigma$ = 84 ppm) compared to the 'Manufacturer' method ($2\sigma$ = 79 ppm) (Figure 3a; Figure 6a; Table 2) when processing the same spectra.

The design of the '18 Fe' mode aims to counteract these effects. A Fe-coated secondary source was explicitly built to decrease the Fe signal, limiting the Fe escape peak drastically. It is unknown whether using a pXRF in which the escape peaks are not automatically corrected (e.g. XMET or Tracer) would improve or degrade the fitting. Uncorrected escape peaks would have to be fitted, and this would also affect the data processing steps. PyMCA implements an escape peak fitting capability that would make this kind of evaluation possible (Solé et al., 2007; Schoonjans et al., 2013). Also, by decreasing the energy of the pXRF emission from the Cu K lines to the Fe K lines, Sc ionisation is improved. Consequently, the '18 Fe' mode provides a better signal to noise ratio on the Sc-K$\alpha$ line (Figure 6b and Figure 7b; Figure F in Supplementary materials). Other modes using lower voltages (7 and 8 kV) without a secondary source were also tested but led to a much higher Ca emission, masking the Sc signal. This observation highlights the importance of the nature of beam conditions, namely tube voltage and secondary source, to quantify elements of interest.

***Spectral interference management***

This study demonstrates that substantial Ca concentrations result in overestimating the Sc content when using the manufacturer method. The calcium/scandium spectral interference effect is shown in ($Sc_{whole\ rock}$ - Sc) vs Ca/Sc diagrams (Figure 4). At low Ca/Sc, sets of eight measurements performed

ACCEPTED MANUSCRIPT

Downloaded from http://geea.lyellcollection.org/ by GSL Maintenance User on July 26, 2021

on a single sample align almost vertically. This kind of subvertical alignment results from the inherent dispersion of the Sc estimates around the average value, while the Ca to Sc ratio (horizontal axis) is correctly evaluated. Moreover, the dispersion along the vertical axis is spread around a zero value, which means that the average of the eight Sc measurements is close to the whole-rock Sc concentration. At high Ca/Sc, sets of eight measurements performed on a single sample align along inclined trends. The inherent dispersion of the Sc estimates is still visible as a variation along the vertical axis but is no longer centred on a correctly estimated average value. These measurements are found at negative $Sc_{whole\ rock} - Sc_{manufacturer}$ values, which means that the pXRF overestimates Sc concentrations in these samples. The trends show a positive slope which means that most overestimated Sc concentrations plot at lower Ca/Sc ratios. Thus, part of the Ca signal in the ROI is considered as Sc by the quantification procedure. The same effect with inclined trends at high Ca/Sc ratios remains visible on the '20 Cu' and '18 Fe' methods. Still, the dispersion along the vertical axis remains spread around a zero value, which means that the average of the eight Sc measurements is close to the whole-rock Sc concentration. The 'manufacturer' quantification method provides accurate Sc values below a Ca/Sc ratio of 67. Both the '20 Cu' and '18 Fe' methods provide reliable Sc estimates at higher Ca/Sc ratios. One sample in the 'Manufacturer' method and another in the '18-Fe' method do not show correctly evaluated Sc concentrations while plotting in the field of the reliable data. Such a result remains compatible with a 2σ interval meaning that 95% of the calculated values are correctly evaluated.

The three methods exposed in the present study require increasing skills in data processing and tuning of analytical conditions. It is easier to use the device's data than reprocessing spectra. It is easier to use the analytical conditions provided by the manufacturer than to change the tube voltage and choose the best-adapted secondary source. The efforts required for data acquisition or processing depends on the kind of limitations encountered during the measurements. If the Sc concentration is high enough but suffers from a high Ca signal Interference, then only data

ACCEPTED MANUSCRIPT

Downloaded from http://geea.lyellcollection.org/ by GSL Maintenance User on July 26, 2021

reprocessing is required. If the Sc concentration is low and the limit of determination needs to be improved, then the analytical conditions have to be modified.

In methods '20 Cu' and '18 Fe', standards with more than 84 and 50 ppm of Sc, respectively, and higher Ca/Sc ratios than those available from the chosen geological context could have given the position of Limit 1 and provided the field in which any results may or may not be reliable. This field may be present on the diagrams shown in Figure 7 as Limit 1 is below Limit 2. Hence, while building a solution to use this method, a standard needs to be found or constructed containing the element of interest above its limit of determination (here Sc) and with an excess of the highly concentrated interfering chemical element (here Ca).

## Conclusion

Scandium analysis in iron oxides using pXRF is a challenge due to low concentrations close to the limit of determination and matrix effects. However, when deconvoluting spectral interferences and taking escape peaks and manufacturer data into account, the potential of pXRF is more significant than initially thought. Therefore, a new method has been developed to quickly assess whether a trace element analysis is valid within an acceptable error range when the matrix contains a spectrally interfering major element.

Specifically, four steps are required: i) select a set of standards covering the expected concentration range of the major and trace element, ii) determine LoDs and calibration lines for major and trace elements, iii) use a diagram that provides the major/trace threshold ratios below which the trace element values are correct, and iv) use the threshold values (LoDs, Limit 1 and Limit 2) to assess whether the values obtained for unknown samples are reliable or not. This step is applicable regardless of the chosen method (i.e., manufacturer or spectral decomposition with or without tuning the experimental conditions). After measuring the standards and processing their data, all values can be read on the device screen as user-defined calibration lines can be implemented and element ratios can be defined in reference. The unexpected outcome of this study is that this

ACCEPTED MANUSCRIPT

Downloaded from http://geea.lyellcollection.org/ by GSL Maintenance User on July 26, 2021

procedure requires at least one standard with Sc above LoD and a Ca/Sc ratio too high to allow an accurate quantification. It therefore requires a standard (material of precisely known concentrations) that cannot be adequately measured by the device. Nevertheless, it is the only solution that delimits the field of 'samples that may or may not be correctly quantified'.

A careful analysis of spectra may significantly improve the confidence and the field of application for pXRF measurements. Furthermore, the processing steps described in this study can be automated. This kind of approach can be applied to any type of interfering emission line. It can be implemented for repetitive tasks and used as test study without requiring new quantification programmes from the pXRF manufacturer. Testing the Fe-Kβ/Co-Kα interference for Ni-bearing laterites would also benecessary, as Co is an economically attractive by-product in such deposits.

Acknowledgements

We thank Mathieu Bauer from Niton Europe, who provided us with the NDT Alpha software and some information on the Xl3t internal features. We also thank Gwendy Hall and Cameron Adams for their detailed and helpful reviews. This work was funded and logistically supported by the French National Research Agency through the 'Investissements d'avenir' national programme of the Labex Ressources 21 with the reference ANR-10-LABX-21-RESSOURCES21 and by the National Centre for Technological Research CNRT 'Nickel et son Environnement' based in Nouméa, New Caledonia (Project grant: 8PS2013-CNRT.CNRS/SCANDIUM). In addition, the authors would like to thank Dr Brice Sevin and Dr Bernard Robineau from the Geological Survey of New Caledonia, together with France Bailly and Laurence Barriller from the National Centre for Technological Research, for their technical and logistical support as well as for sharing their extensive knowledge of the geology of New Caledonia. We are grateful to Société Le Nickel (SLN), Koniambo Nickel SAS (KNS), Nickel Mining Company (NMC), Société des Mines de la Tontouta (SMT) and Mai Kouaoua Mines (MKM) for support and access to mines and drill cores. We also thank Dr. Christophe Cloquet (SARM analytical

ACCEPTED MANUSCRIPT

Downloaded from http://geea.lyellcollection.org/ by GSL Maintenance User on July 26, 2021

centre, CRPG, Vandœuvre-lès-Nancy, France) and Pabla Antonini (GeoRessources, Vandœuvre-lès-Nancy, France) for technical support in providing analytical data.

Declaration of interest

None

References

Adams, C., Brand, C., Dentith, M., Fiorentini, M., Caruso, S., Mehta, M., 2020. The use of pXRF for light element geochemical analysis: a review of hardware design limitations and an empirical investigation of air, vacuum, helium flush and detector window technologies. Geochemistry: Exploration, Environment, Analysis 20, 366–380. https://doi.org/10.1144/geochem2019-076

Andrew, B.S., Barker, S.L.L., 2018. Determination of carbonate vein chemistry using portable X-ray fluorescence and its application to mineral exploration. Geochemistry: Exploration, Environment, Analysis 18, 85–93. https://doi.org/10.1144/geochem2016-011

Arantes de Carvalho, G.G., Bueno Guerra, M.B., Adame, A., Nomura, C.S., Oliveira, P.V., Pereira de Carvalho, H.W., Santos, D., Nunes, L.C., Krug, F.J., 2018. Recent advances in LIBS and XRF for the analysis of plants. J. Anal. At. Spectrom. 33, 919–944. https://doi.org/10.1039/C7JA00293A

Arne, D.C., Mackie, R.A., Jones, S.A., 2014. The use of property-scale portable X-ray fluorescence data in gold exploration: advantages and limitations. Geochemistry: Exploration, Environment, Analysis 14, 233–244. https://doi.org/10.1144/geochem2013-233

Audet, M.-A., 2008. Le massif du Koniambo - Nouvelle Calédonie : Formation et obduction d'un complexe ophiolitique de type SSZ. Enrichissement en nickel, cobalt et scandium dans les profils résiduels. (Sciences de la Terre). Université de Nouvelle Calédonie, Nouvelle Calédonie,.

ACCEPTED MANUSCRIPT

Downloaded from http://geea.lyellcollection.org/ by GSL Maintenance User on July 26, 2021

Beckhoff, B., Kanngiesser, B., Langhoff, N., Wedell, R., Wolff, H., 2006. Handbook of practical X-ray fluorescence analysis. Springer, Berlin; New York.

Brand, N.W., Brand, C.J., 2014. Performance comparison of portable XRF instruments. Geochemistry: Exploration, Environment, Analysis 14, 125–138. https://doi.org/10.1144/geochem2012-172

Cao, Y.H., Linnen, R.L., Good, D.J., Samson, I.M., Epstein, R., 2016. The application of portable XRF and benchtop SEM-EDS to Cu-Pd exploration in the Coldwell Alkaline Complex, Ontario, Canada. Geochemistry: Exploration, Environment, Analysis 16, 193–212. https://doi.org/10.1144/geochem2015-394

Carignan, J., Hild, P., Mevelle, G., Morel, J., Yeghicheyan, D., 2001. Routine Analyses of Trace Elements in Geological Samples using Flow Injection and Low Pressure On-Line Liquid Chromatography Coupled to ICP-MS: A Study of Geochemical Reference Materials BR, DR-N, UB-N, AN-G and GH. Geostandards and Geoanalytical Research 25, 187–198. https://doi.org/10.1111/j.1751-908X.2001.tb00595.x

Cauzid, J., 2005. Geochimie et Imagerue X des Fluides inclus dans les systemes Hydrothermaux Fossiles: Developpements Experimentaux (Geochimie Fondamentale et Appliquée). Université Paris 7, Paris.

Cluzel, D., Aitchison, J., Picard, C., 2001. Tectonic accretion and underplating of mafic terranes in the Late Eocene intraoceanic fore-arc of New Caledonia (Southwest Pacific): geodynamic implications (Tectonophysics, Elsevier 340).

Conrey, R.M., Goodman-Elgar, M., Bettencourt, N., Seyfarth, A., Van Hoose, A., Wolff, J.A., 2014. Calibration of a portable X-ray fluorescence spectrometer in the analysis of archaeological samples using influence coefficients. Geochemistry: Exploration, Environment, Analysis 14, 291–301. https://doi.org/10.1144/geochem2013-198

ACCEPTED MANUSCRIPT

Downloaded from http://geea.lyellcollection.org/ by GSL Maintenance User on July 26, 2021

Fisher, L., Gazley, M.F., Baensch, A., Barnes, S.J., Cleverley, J., Duclaux, G., 2014. Resolution of geochemical and lithostratigraphic complexity: a workflow for application of portable X-ray fluorescence to mineral exploration. Geochemistry: Exploration, Environment, Analysis 14, 149–159. https://doi.org/10.1144/geochem2012-158

Frahm, E., 2017. First hands-on tests of an Olympus Vanta portable XRF analyzer to source armenian obsidian artefacts. International Association for Obsidian Studies 8–23.

Gallhofer, D., Lottermoser, B., 2018. The Influence of Spectral Interferences on Critical Element Determination with Portable X-Ray Fluorescence (pXRF). Minerals 8, 320. https://doi.org/10.3390/min8080320

Gazley, M.F., Bonnett, L.C., Fisher, L.A., Salama, W., Price, J.H., 2017. A workflow for exploration sampling in regolith-dominated terranes using portable X-ray fluorescence: comparison with laboratory data and a case study. Australian Journal of Earth Sciences 64, 903–917. https://doi.org/10.1080/08120099.2017.1367721

Gazley, M F, Duclaux, G., Fisher, L.A., de Beer, S., Smith, P., Taylor, M., Swanson, R., Hough, R.M., Cleverley, J.S., 2011. 3D visualisation of portable X-ray fluorescence data to improve geological understanding and predict metallurgical performance at Plutonic Gold Mine, Western Australia. Applied Earth Science 120, 88–96. https://doi.org/10.1179/1743275812Y.0000000002

Gazley, M.F., Fisher, L.A., 2014. A review of the reliability and validity of portable X-ray fluorescence spectrometry (pXRF) data, in: Mineral Resource and Ore Reserve Estimation - The AusIMM Guide to Good Practice (2nd Ed), Mineral Resource and Ore Reserve. AusIMM, Melbourne, pp. 1–13.

ACCEPTED MANUSCRIPT

Downloaded from http://geea.lyellcollection.org/ by GSL Maintenance User on July 26, 2021

Gazley, M.F., Vry, J.K., du Plessis, E., Handler, M.R., 2011. Application of portable X-ray fluorescence analyses to metabasalt stratigraphy, Plutonic Gold Mine, Western Australia. Journal of Geochemical Exploration 110, 74–80. https://doi.org/10.1016/j.gexplo.2011.03.002

Gisbert, G., Tornos, F., Losantos, E., Pons, J.M., Videira, J.C., 2021. Vectors to ore in replacive VMS deposits of the northern Iberian Pyrite Belt: mineral zoning, whole rock geochemistry, and use of portable XRF (preprint). The evolving Earth surface/Geochemistry, mineralogy, petrology, and volcanology/Geochemistry. https://doi.org/10.5194/se-2021-50

Glanzman, R.K., Closs, L.G., 2007. Field Portable X-Ray Fluorescence Geochemical Analysis – Its Contribution to Onsite Real-time Project Evaluation, in: Environmental Science, Advances in Prospect-Scale Geochemical Methods. Presented at the Proceedings of Exploration 07: Fifth Decennial International Conference on Mineral Exploration, B. Milkereit, Toronta, Canada, pp. 291–301.

Hall, G.E.M., Bonham-Carter, G.F., Buchar, A., 2014. Evaluation of portable X-ray fluorescence (pXRF) in exploration and mining: Phase 1, control reference materials. Geochemistry: Exploration, Environment, Analysis 14, 99–123. https://doi.org/10.1144/geochem2013-241

Hall, G.E.M., McClenaghan, M.B., Pagé, L., 2016. Application of portable XRF to the direct analysis of till samples from various deposit types in Canada. Geochemistry: Exploration, Environment, Analysis 16, 62–84. https://doi.org/10.1144/geochem2015-371

Hughes, R., Barker, S.L.L., 2018. Using portable XRF to infer adularia halos within the Waihi Au-Ag system, New Zealand. Geochemistry: Exploration, Environment, Analysis 18, 97–108. https://doi.org/10.1144/geochem2016-006

Ibáñez-Insa, J., Pérez-Cano, J., Fondevilla, V., Oms, O., Rejas, M., Fernández-Turiel, J.L., Anadón, P., 2017. Portable X-ray fluorescence identification of the Cretaceous–Paleogene boundary:

ACCEPTED MANUSCRIPT

Downloaded from http://geea.lyellcollection.org/ by GSL Maintenance User on July 26, 2021

Application to the Agost and Caravaca sections, SE Spain. Cretaceous Research 78, 139–148. https://doi.org/10.1016/j.cretres.2017.06.004

Kim, H.-R., Kim, K.-H., Yu, S., Moniruzzaman, M., Hwang, S.-I., Lee, G.-T., Yun, S.-T., 2019. Better assessment of the distribution of As and Pb in soils in a former smelting area, using ordinary co-kriging and sequential Gaussian co-simulation of portable X-ray fluorescence (PXRF) and ICP-AES data. Geoderma 341, 26–38. https://doi.org/10.1016/j.geoderma.2019.01.031

Konstantinov, M.M., Strujkov, S.F., 1995. Application of indicator halos (signs of ore remobilization) in exploration for blind gold and silver deposits. Journal of Geochemical Exploration 54, 1–17. https://doi.org/10.1016/0375-6742(95)00003-8

Lachance, G.R., Claisse, F., 1995. Quantitative X-ray fluorescence analysis: theory and application, First edition. ed. Wiley, Chichester ; New York.

Laperche, V., 2005. Evaluation des performances du spectromètre portable de fluorescence X Niton XL723S (au laboratoire et sur le terrain). (Public report No. RP-533377-FR). BRGM, Orléans.

Le Vaillant, M., Barnes, S.J., Fisher, L., Fiorentini, M.L., Caruso, S., 2014. Use and calibration of portable X-Ray fluorescence analysers: application to lithogeochemical exploration for komatiite-hosted nickel sulphide deposits. Geochemistry: Exploration, Environment, Analysis 14, 199–209. https://doi.org/10.1144/geochem2012-166

Lemière, B., 2018. A review of pXRF (field portable X-ray fluorescence) applications for applied geochemistry. Journal of Geochemical Exploration 188, 350–363. https://doi.org/10.1016/j.gexplo.2018.02.006

Lemiere, B., Laperche, V., Haouche, L., Auger, P., 2014. Portable XRF and wet materials: application to dredged contaminated sediments from waterways. Geochemistry: Exploration, Environment, Analysis 14, 257–264. https://doi.org/10.1144/geochem2012-179

ACCEPTED MANUSCRIPT

Downloaded from http://geea.lyellcollection.org/ by GSL Maintenance User on July 26, 2021

Margui, E., Van Grieken, R., 2013. X-Ray Fluorescence Spectrometry and Related Techniques, 1st ed. Momentum Press, New York. https://doi.org/10.5643/9781606503935

Menez, B., 1999. Les microsondes photo et protons appliquées à l'analyse ponctuelle d'inclusions fluides : un outil pour reconstituer l'évolution des paléosystèmes hydrothermaux. Université Paris 7, Paris.

Mussini, J.-M., 2009. Mesures expérimentales et simulation Monte Carlo de la fonction de réponse d'un détecteur Si(Li) : application à l'analyse quantitative multi-élémentaire par XRF et PIXE (Physique Nucléaire Théorique [nucl-th]). Université de Strasbourg, Strasbourg.

Piercey, S.J., Devine, M.C., 2014. Analysis of powdered reference materials and known samples with a benchtop, field portable X-ray fluorescence (pXRF) spectrometer: evaluation of performance and potential applications for exploration lithogeochemistry. Geochemistry: Exploration, Environment, Analysis 14, 139–148. https://doi.org/10.1144/geochem2013-199

Quiniou, T., Laperche, V., 2014. An assessment of field-portable X-ray fluorescence analysis for nickel and iron in laterite ore (New Caledonia). Geochemistry: Exploration, Environment, Analysis 14, 245–255. https://doi.org/10.1144/geochem2012-159

Ribeiro, B.T., Silva, S.H.G., Silva, E.A., Guilherme, L.R.G., 2017. Portable X-ray fluorescence (pXRF) applications in tropical Soil Science. Ciênc. agrotec. 41, 245–254. https://doi.org/10.1590/1413-70542017413000117

Ross, P.-S., Bourke, A., Fresia, B., 2014. Improving lithological discrimination in exploration drill-cores using portable X-ray fluorescence measurements: (1) testing three Olympus Innov-X analysers on unprepared cores. Geochemistry: Exploration, Environment, Analysis 14, 171–185. https://doi.org/10.1144/geochem2012-163

Ryan, C.G., Clayton, E., Griffin, W.L., Sie, S.H., Cousens, D.R., 1988. SNIP, a statistics-sensitive background treatment for the quantitative analysis of PIXE spectra in geoscience

ACCEPTED MANUSCRIPT

Downloaded from http://geea.lyellcollection.org/ by GSL Maintenance User on July 26, 2021

applications. Nuclear Instruments and Methods in Physics Research Section B: Beam Interactions with Materials and Atoms 34, 396–402. https://doi.org/10.1016/0168-583X(88)90063-8

Sanoit (de), J., Chambellan, D., Plassard, F., 2005. Caractérisation in situ du pigment noir de quelques oeuvres pariétales de la Grotte de Rouffignac à l'aide d'un système portable d'analyse par fluorescence X (XRF). archeosciences 61–68. https://doi.org/10.4000/archeosciences.614

Sarala, P., 2016. Comparison of different portable XRF methods for determining till geochemistry. Geochemistry: Exploration, Environment, Analysis 16, 181–192. https://doi.org/10.1144/geochem2012-162

Schoonjans, T., Solé, V.A., Vincze, L., Sanchez del Rio, M., Appel, K., Ferrero, C., 2013. A general Monte Carlo simulation of energy-dispersive X-ray fluorescence spectrometers — Part 6. Quantification through iterative simulations. Spectrochimica Acta Part B: Atomic Spectroscopy 82, 36–41. https://doi.org/10.1016/j.sab.2012.12.011

Shao, J., Jia, W., Zhang, X., Liu, Y., Tang, X., Xiong, G., Shan, Q., 2020. Analysis of plant samples by low-power total reflection X-ray fluorescence spectrometry applying argon-peak normalization. J. Anal. At. Spectrom. 35, 746–753. https://doi.org/10.1039/C9JA00419J

Sitko, R., Zawisza, B., 2012. Chapter 8: Quantification in X-Ray Fluorescence Spectrometry, in: X-RAY SPECTROSCOPY. IntechOpen, pp. 137–162.

Solé, V.A., Papillon, E., Cotte, M., Walter, Ph., Susini, J., 2007. A multiplatform code for the analysis of energy-dispersive X-ray fluorescence spectra. Spectrochimica Acta Part B: Atomic Spectroscopy 62, 63–68. https://doi.org/10.1016/j.sab.2006.12.002

Statham, P.J., 1976. A comparative study of techniques for quantitative analysis of the X-ray spectra obtained with a Si(Li) detector. X-Ray Spectrom. 5, 16–28. https://doi.org/10.1002/xrs.1300050106

ACCEPTED MANUSCRIPT

Downloaded from http://geea.lyellcollection.org/ by GSL Maintenance User on July 26, 2021

Teitler, Y., Cathelineau, M., Ulrich, M., Ambrosi, J.P., Munoz, M., Sevin, B., 2019. Petrology and geochemistry of scandium in New Caledonian Ni-Co laterites. Journal of Geochemical Exploration 196, 131–155. https://doi.org/10.1016/j.gexplo.2018.10.009

Thompson, A., Attwood, D., Gullikson, E., Howells, M., Kortright, J., Robinson, A., Underwood, J., Kim, K., Kwang, K., Lindau, L., Pianetta, P., Winick, H., Williams, G., Scofield, J., Vaughan, D., 2001. X-RAY DATA BOOKLET, National Laboratory. ed. Lawrence Berkeley National Laboratory, Berkeley, California 94720.

Tian, K., Huang, B., Xing, Z., Hu, W., 2018. In situ investigation of heavy metals at trace concentrations in greenhouse soils via portable X-ray fluorescence spectroscopy. Environ Sci Pollut Res 25, 11011–11022. https://doi.org/10.1007/s11356-018-1405-8

Tian, L., Zhu, J., Liu, M., An, Z., 2009. Bremsstrahlung spectra produced by kilovolt electron impact on thick targets. Nuclear Instruments and Methods in Physics Research Section B: Beam Interactions with Materials and Atoms 267, 3495–3499. https://doi.org/10.1016/j.nimb.2009.08.009

Ulrich, M., Cathelineau, M., Munoz, M., Boiron, M.C., Karpoff, A.M., 2019. The relative distribution of critical (Sc, REE) and transition metals (Ni, Co, Cr, Mn, V) in some Ni-laterite deposits of New Caledonia. J. Geochemical Exploration 197, 93–113.

Ulrich, M., Muñoz, M., Boulvais, P., Cathelineau, M., Cluzel, D., Guillot, S., Picard, C., 2020. Serpentinization of New Caledonia peridotites: from depth to (sub-)surface. Contrib Mineral Petrol 175, 91. https://doi.org/10.1007/s00410-020-01713-0

Van Espen, P., Nullens, H., Adams, F., 1980. An in-depth study of energy-dispersive x-ray spectra. X-Ray Spectrom. 9, 126–133. https://doi.org/10.1002/xrs.1300090308

ACCEPTED MANUSCRIPT

Downloaded from http://geea.lyellcollection.org/ by GSL Maintenance User on July 26, 2021

Whiting, E.E., 1968. An empirical approximation to the Voigt profile. Journal of Quantitative Spectroscopy and Radiative Transfer 8, 1379–1384. https://doi.org/10.1016/0022-4073(68)90081-2

Young, K.E., Evans, C.A., Hodges, K.V., Bleacher, J.E., Graff, T.G., 2016. A review of the handheld X-ray fluorescence spectrometer as a tool for field geologic investigations on Earth and in planetary surface exploration. Applied Geochemistry 72, 77–87. https://doi.org/10.1016/j.apgeochem.2016.07.003

Table captions

Table 1: Sample excitation conditions and data processing techniques of the three methods used in this study (namely 'Manufacturer', '20 Cu' and '18 Fe').

Figure captions

**Figure 1: Comparison of an XRF spectrum (log scale of counts per second as a function of energy in keV) fitted with PyMCA (Solé et al., 2007) for the same laterite sample (e.g. sample containing 2.0% of Ca and 192.9 ppm of Sc) acquired with two pXRF spectrometers. Energy range from 1 to 8 keV in which several artefacts encountered in XRF spectrometry is visible**:

*(A) Spectrum acquired with the Niton Xl3t GOLDD+ pXRF (Ag anode) ; (B) Spectrum acquired with the XMET® 7500 pXRF (Rh anode) and (C) Zoom of spectrum acquired with the XMET® pXRF from 3.6 to 4.8 keV showing the artefacts that can disrupt the scandium quantification such as spectral interferences and escape peaks (Ca-Kα/escape_Cr-Kα; Ca-Kβ/Sc-Kα/escape_Mn-Kα; Ti-Kα/ Sc-Kβ/escape-Fe-Kα) where a is the Ca-K$\beta$ emission line, b is the Sc-K$\alpha$ emission-line, c is the escape peak of the Mn-K$\alpha$ emission line, d is the Sc-K$\beta$ emission line, e is the Ti-K$\alpha$ emission line and f the escape peak of the Fe-K$\alpha$ emission line. In addition, a Niton automatically corrects the escape peak of Fe on spectrum while the XMET does not. The automatic correction is seen as a downward peak on the Niton.*

ACCEPTED MANUSCRIPT

Downloaded from http://geea.lyellcollection.org/ by GSL Maintenance User on July 26, 2021

**Figure 2: Distribution of analysed samples in a Ca-Sc biplot.**

*Diamonds represent real samples; squares are samples made from a weighted mixture of two samples. Red symbols correspond to samples considered as 'standards' and black symbols to 'unknown samples'.*

**Figure 3: Calibration lines for Sc (a) and Ca (b) with the 'Manufacturer' method.**

*Diamonds with black edges correspond to the 11 standards used to build the calibration line. Diamonds without an edge line correspond to the samples used for checking the calculated calibration line. Blue diamonds correspond to standards or samples for which the average of their eight measurements falls within ±2$\sigma$ from the calibration line. Red diamonds correspond to standards or samples for which the average of their eight measurements falls outside of the ±2$\sigma$ interval from the calibration line.*

**Figure 4: Threshold values of the Ca/Sc apparent concentration. The ratio defined as Limit1 corresponds to a Ca/Sc ratio of 67, under which the Ca-Sc spectral interference is correctly solved. Limit2 corresponds to a Ca/Sc ratio of 104, above which the spectral interference is never solved.**

*Diamonds with black edges correspond to the 11 standards used to build the calibration line. Diamonds without an edge line correspond to the samples used for checking the calculated calibration line. Blue diamonds correspond to standards or samples for which the average of their eight measurements falls within ±2$\sigma$ from the Sc-calibration curve. Red diamonds correspond to standards or samples for which the average of their eight measurements falls outside the ±2$\sigma$ interval.*

**Figure 5: Ca vs Sc biplot obtained with the 'Manufacturer' method.**

*Black dots correspond to whole-rock values and are linked to crosses bracketing minimum and maximum values for Ca, and Sc estimated from pXRF. Thin solid lines are standards. Thin dashed lines are samples. Blue lines correspond to standards or samples for which the average of their eight measurements falls within ±2$\sigma$ around the Sc-calibration curve, and*

ACCEPTED MANUSCRIPT

Downloaded from http://geea.lyellcollection.org/ by GSL Maintenance User on July 26, 2021

*red lines correspond to standards or samples for which the average of their eight measurements falls outside the ±2σ interval around the Sc-calibration curve. The bold, vertical green line corresponds to the LoD of Sc (79 ppm). Bold dashed green lines correspond to Limit 1 (under which Sc values are correctly evaluated; Ca/Sc = 67) and Limit 2 (above which Sc values have never been accurately assessed; Ca/Sc = 104).*

**Figure 6: Calibration lines obtained with the '20 Cu' (a) and '18 Fe' (b) methods.**

*Diamonds with black edges correspond to the 11 standards used to build the calibration line. Diamonds without an edge line correspond to the samples used for checking the calculated calibration line. Blue diamonds correspond to standards or samples for which the average of their eight measurements falls within ±2σ around the calibration curve. Red diamonds correspond to standards or samples for which the average of their eight measurements falls outside of the ±2σ interval around the calibration curve.*

**Figure 7: Ca vs Sc biplots obtained with the '20 Cu' (A) and '18 Fe' (B) methods.**

*Black dots correspond to whole-rock values and are linked to elongated crosses bracketing minimum and maximum Ca and Sc values. Thin solid lines are standards. Thin dashed lines are samples. Blue lines correspond to standards or samples for which the average of their eight measurements falls within ±2σ around the Sc-calibration curve. Red lines correspond to standards or samples for which the average of their eight measurements falls outside the ±2σ interval around the Sc-calibration curve. Bold vertical black lines correspond to the LoD for Sc (Table 3). Bold solid black lines correspond to the Ca/Sc ratio under which Sc values are correctly evaluated. Bold dashed black lines correspond to the Ca/Sc ratio above which Sc values are never accurately assessed.*

ACCEPTED MANUSCRIPT

Downloaded from http://geea.lyellcollection.org/ by GSL Maintenance User on July 26, 2021

Figure 1

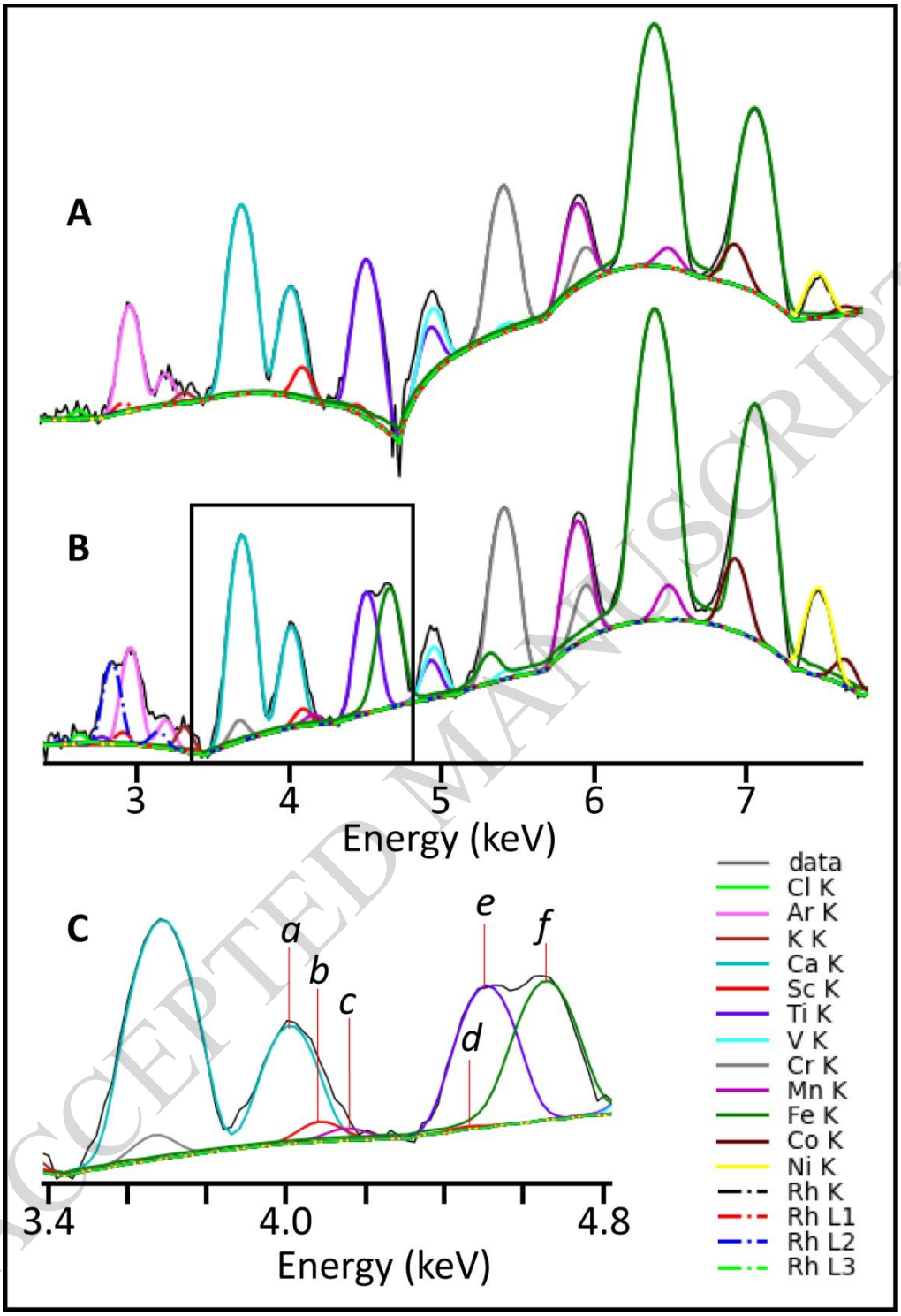


ACCEPTED MANUSCRIPT

Downloaded from http://geea.lyellcollection.org/ by GSL Maintenance User on July 26, 2021

Figure 2

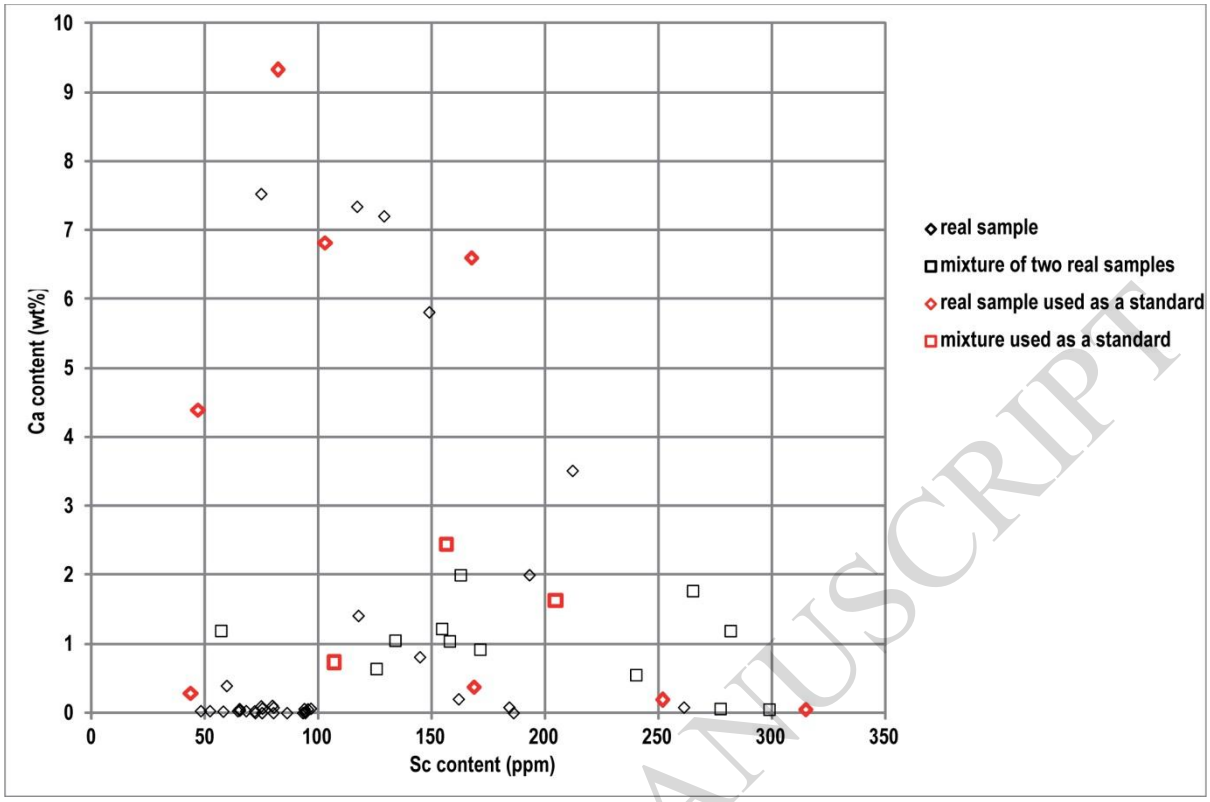


ACCEPTED MANUSCRIPT

Downloaded from http://geea.lyellcollection.org/ by GSL Maintenance User on July 26, 2021

Figure 3

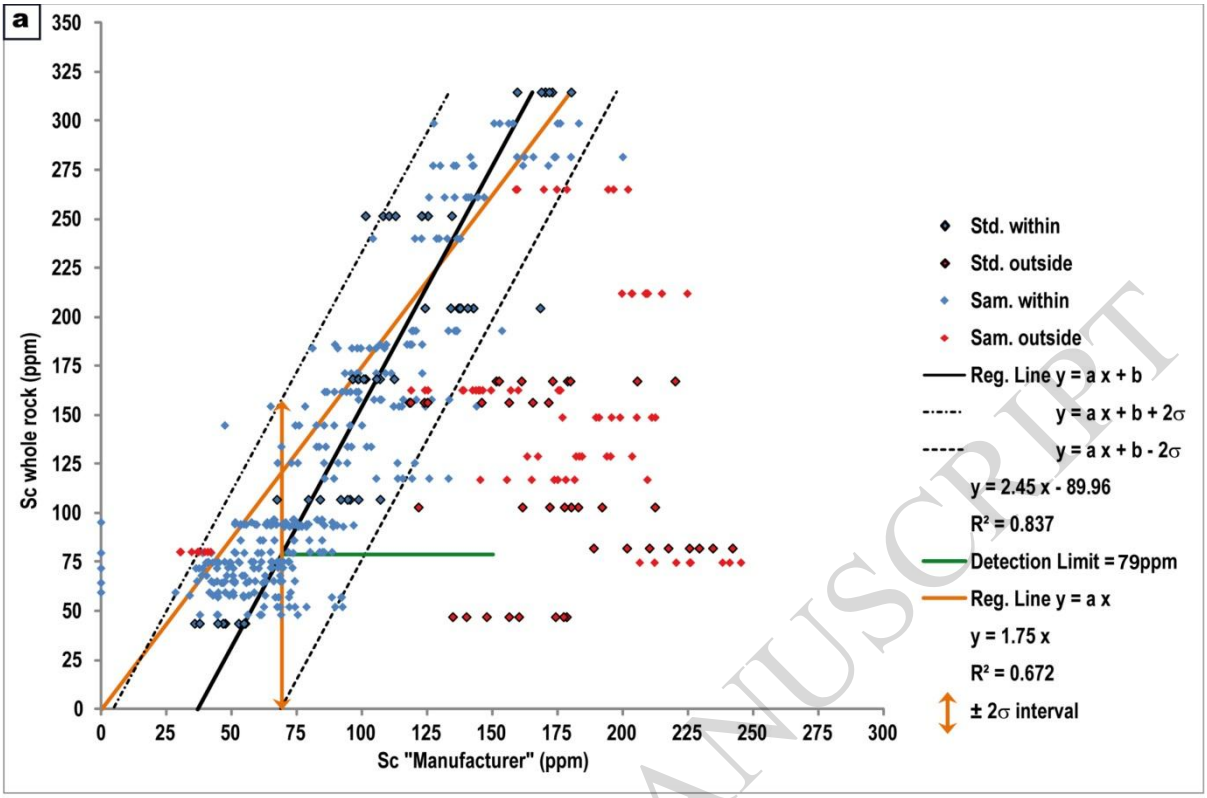


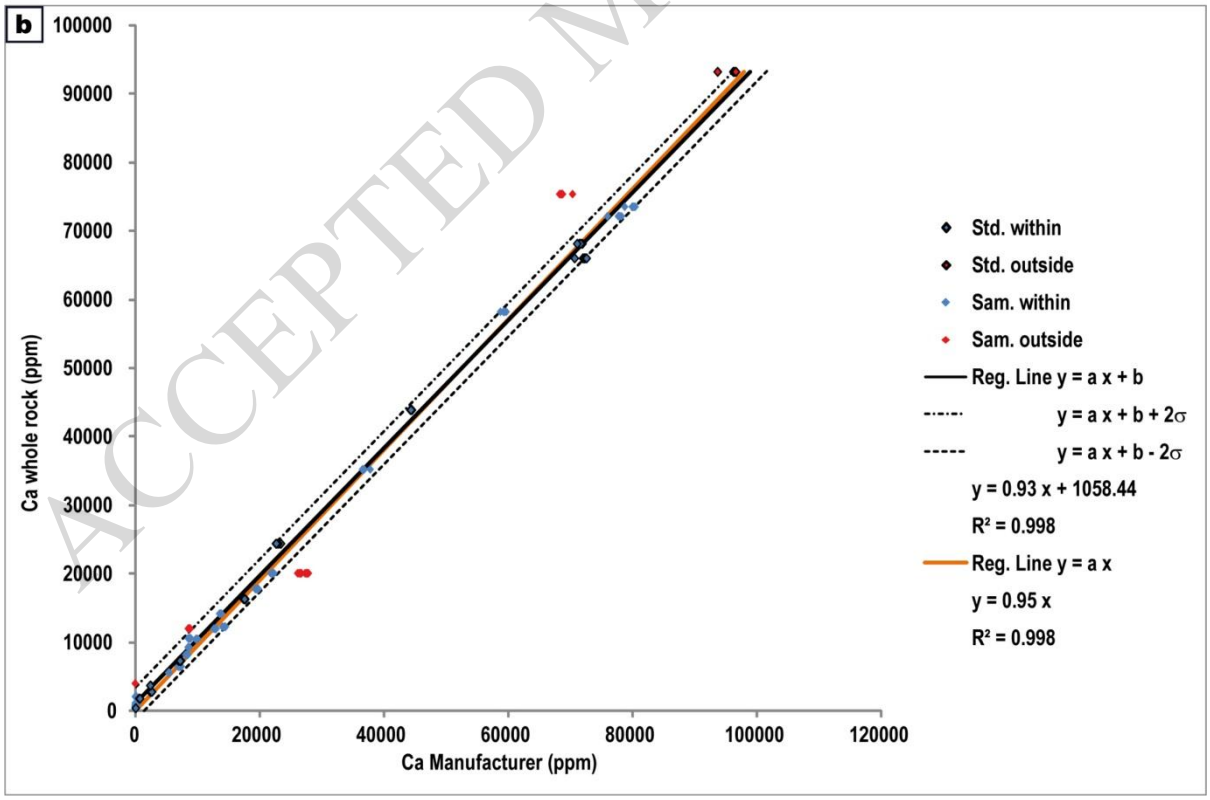


ACCEPTED MANUSCRIPT

Downloaded from http://geea.lyellcollection.org/ by GSL Maintenance User on July 26, 2021

Figure 4

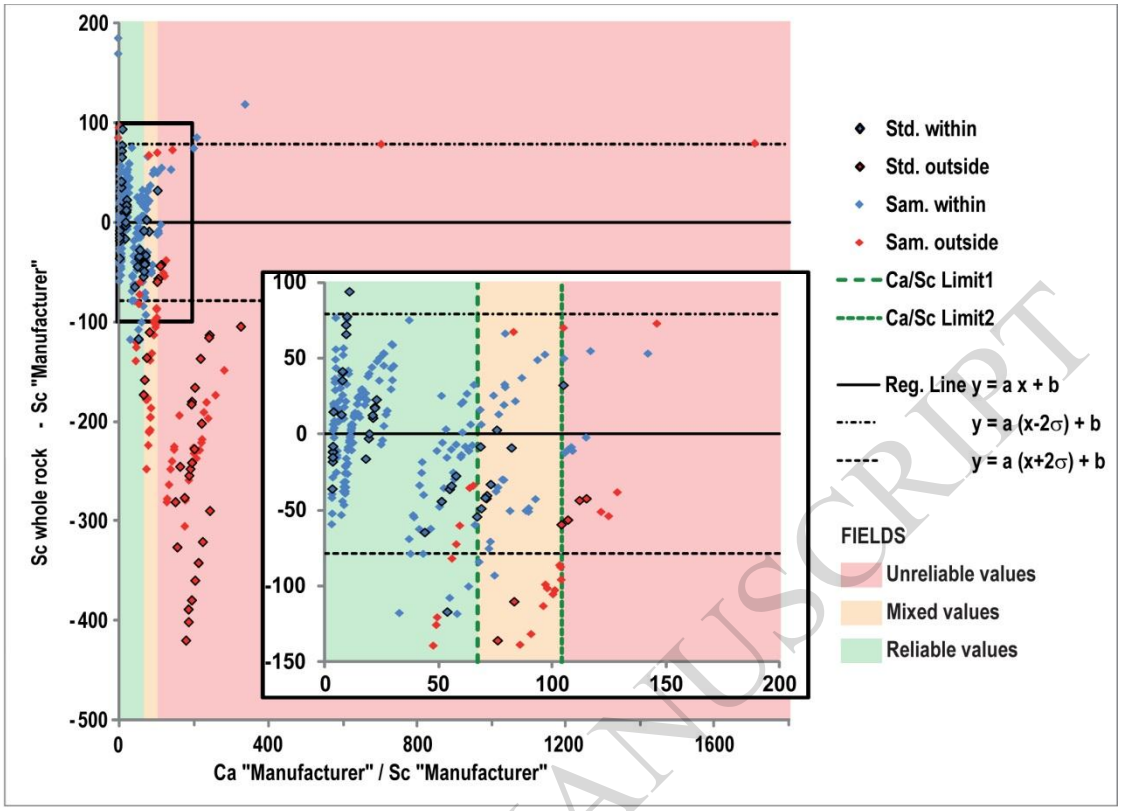


ACCEPTED MANUSCRIPT

Downloaded from http://geea.lyellcollection.org/ by GSL Maintenance User on July 26, 2021

Figure 5

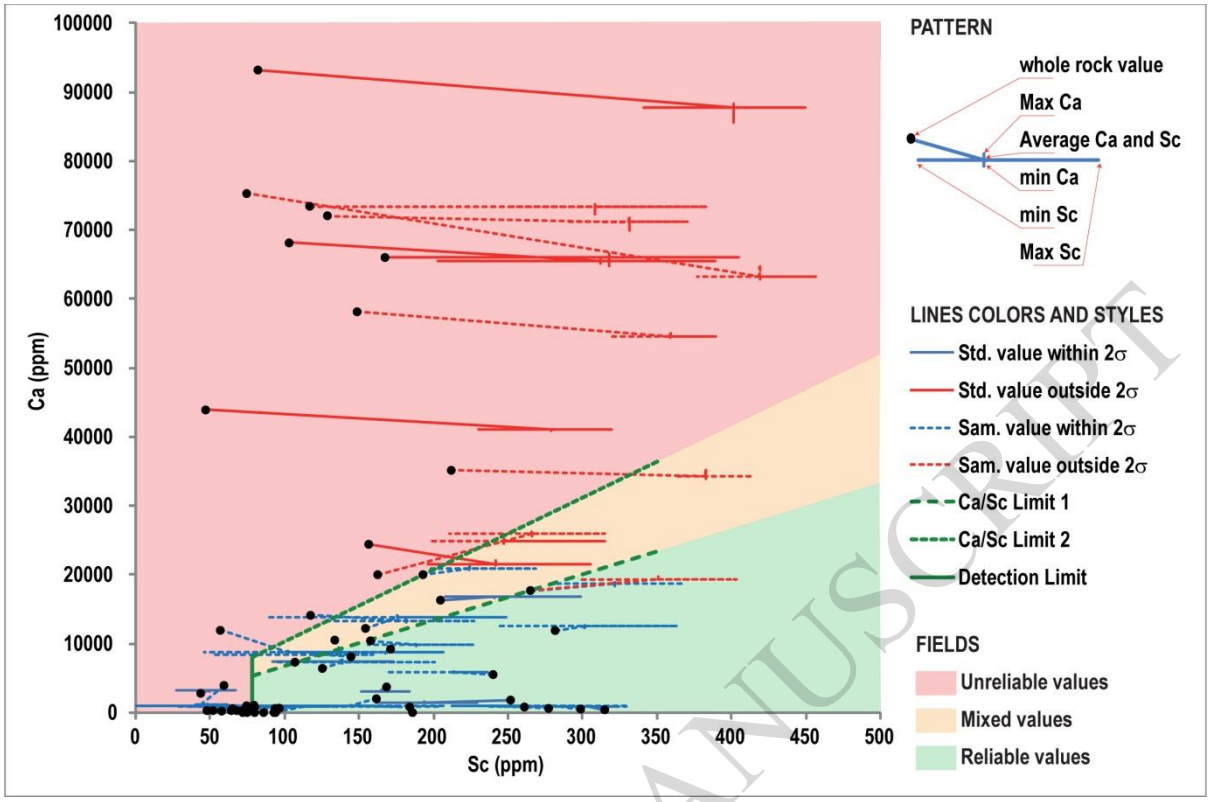


ACCEPTED MANUSCRIPT

Downloaded from http://geea.lyellcollection.org/ by GSL Maintenance User on July 26, 2021

Figure 6

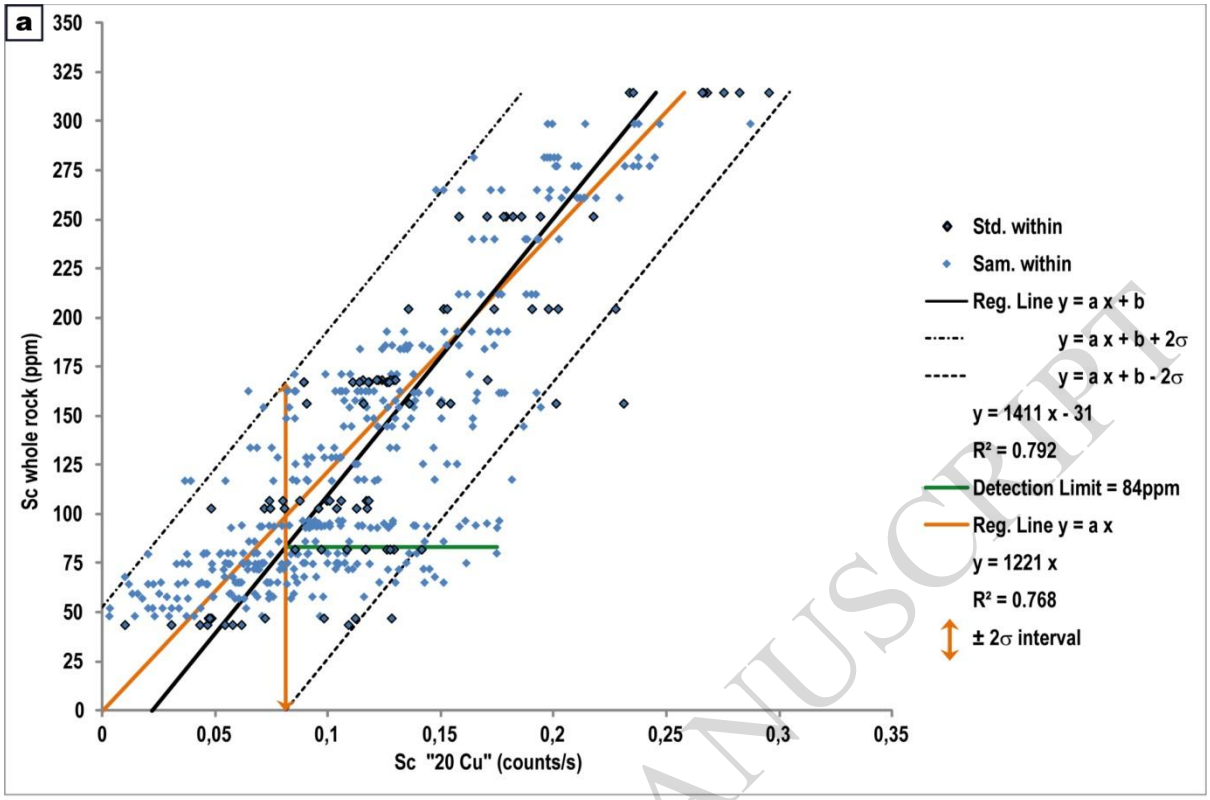


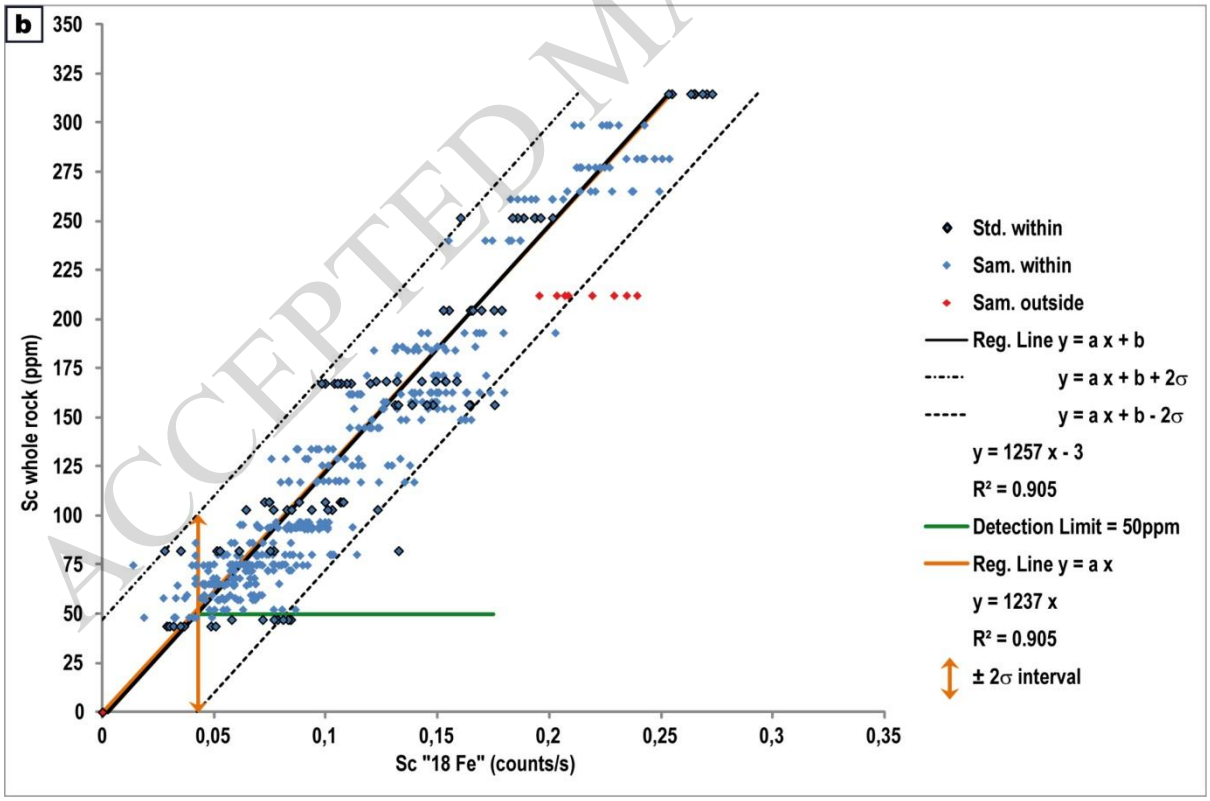


ACCEPTED MANUSCRIPT

Downloaded from http://geea.lyellcollection.org/ by GSL Maintenance User on July 26, 2021

Figure 7

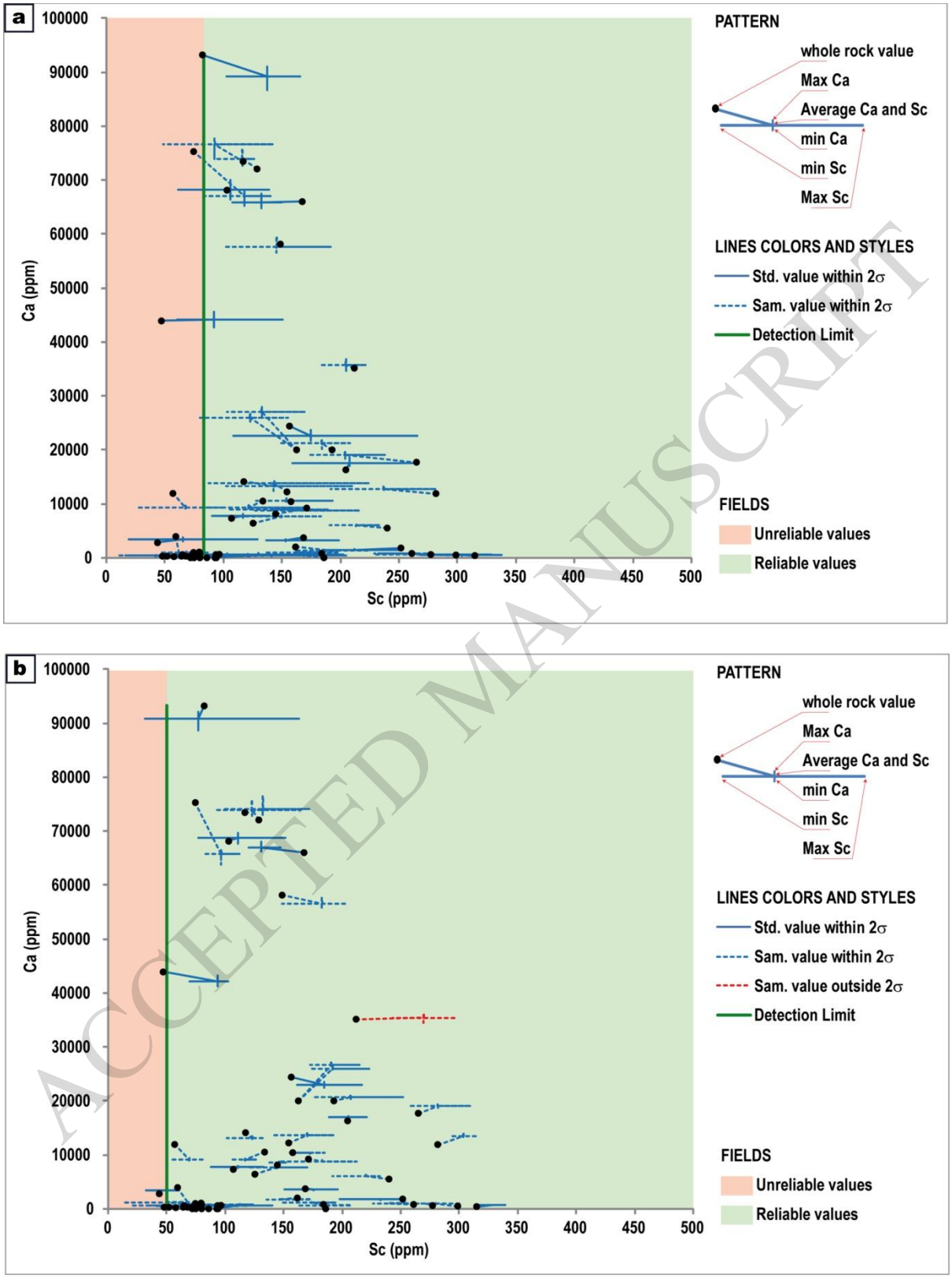


ACCEPTED MANUSCRIPT

| Data processing / Sample excitation | Region of Interest (ROI) | Spectral fitting |
|---|---|---|
| "Low" filter: 20 kV + Cu-coated foil | Manufacturer | 20 Cu |
| In-house filter: 18 kV + Fe-coated foil | - | 18 Fe |

ACCEPTED MANUSCRIPT